the loss of constitutive expression in the Nrf2 KO mice. It remains to be established whether a functional ARE exists further upstream of the 5′-flanking region that was described by Reinhart and Pearson [42]. The alternative possibility that BHA induction of *Gstm3* is regulated indirectly by Nrf2 also cannot be discounted. According to this hypothesis, Nrf2 would affect induction of transcription factors that are regulated through ARE enhancers. Such examples could include c-Jun, JunB, ATF3 or ATF4, since they have been reported to be induced by tBHQ [46,47]. Further investigations are required to test these possibilities.

Class Pi *Gstp1* and *Gstp2* are modestly inducible in female mice. The sequence 5′-TTGAGTCAGCA-3′ is found not only between nt −60 and −50 flanking *Gstp1*, but also between nt −71 and −61 flanking *Gstp2* [48,49]. Given the fact that induction of Gstp1, and, to a lesser extent, Gstp2, by BHA is abolished in the KO mice, it seems likely that this putative *cis*-element serves as a recognition site for Nrf2, even though it is not a perfect ARE.

Sex-specific induction

The present study has revealed that BHA is a more potent inducer of many GST genes in the livers of female mice than in the livers of male mice. This finding might be due to some type of co-operative interaction between the oestrogen receptor and Nrf2. Alternatively, BHA may be metabolized in a sex-specific fashion. It could be postulated that t-BHQ accumulates to a greater extent in the livers of female mice than their male counterparts. Sex-specific differences may exist in sulphation or glucuronidation of BHA, or the O-demethylation of BHA to t-BHQ, or the oxidase and GST responsible for conversion of t-BHQ into t-butyl-1,4-benzoquinone and subsequent conjugation with GSH (see [50] for details of biotransformation of BHA). These possibilities warrant investigation.

Concluding comments

TaqMan® real-time PCR has been used to examine the effect of the Nrf2 bZIP transcription on expression of individual antioxidant and/or detoxication genes in a gene KO mouse model. Such assays, along with conventional analytical biochemistry methods, have shown that the constitutive hepatic expression of various class Alpha and class Mu GST, along with expression of GCLC, is reduced significantly in *Nrf2*$^{-/-}$ mice. In *Nrf2*$^{-/-}$ mice, the ability of BHA to affect induction of protein/mRNA appeared to be independent of the changes in constitutive expression affected by the bZIP factor. Our results suggest that the innate loss of hepatic detoxification capacity in the *Nrf2*$^{-/-}$ mouse, as much as failure to elicit an adequate adaptive response, is responsible for the mutant mouse being less able to tolerate chemical and oxidative stress than WT mice. This apparent dissociation between constitutive and inducible expression warrants further investigation.

This work was funded by grants from the Association for International Cancer Research (99-041), the World Cancer Research Fund (2000/11), and the Medical Research Council (G0000281). S.A.C. holds a Co-operative Awards in Science and Engineering Medical Research Council Ph.D. studentship. We thank Dr Christophe Cavin (Nestlé Research Center, Lausanne, Switzerland) for his generosity in providing the cafestol and kahweol palmitate used in the feeding experiments. We also thank Dr Bill Pearson for his helpful expert advice about GST nomenclature, and for providing information about the identity of EST clones. Lastly, we are enormously grateful to Dr Irving Listowsky for his critical comments about GST nomenclature, and for pointing out an error in one of our Gstm4 cDNA clones prior to publication.

REFERENCES

1 Hayes, J. D. and McLellan, L. I. (1999) Glutathione and glutathione-dependent enzymes represent a co-ordinately regulated defence against oxidative stress. Free Radical Res. **31**, 273–300
2 Wild, A. C. and Mulcahy, R. T. (2000) Regulation of γ-glutamylcysteine synthetase subunit gene expression: insights into transcriptional control of antioxidant defences. Free Radical Res. **32**, 281–301
3 Rushmore, T. H., Morton, M. R. and Pickett, C. B. (1991) The antioxidant responsive element. Activation by oxidative stress and identification of the DNA consensus sequence required for functional activity. J. Biol. Chem. **266**, 11632–11639
4 Favreau, L. V. and Pickett, C. B. (1991) Transcriptional regulation of the rat NAD(P)H: quinone reductase gene. Identification of regulatory elements controlling basal level expression and inducible expression by planar aromatic compounds and phenolic antioxidants. J. Biol. Chem. **266**, 4556–4561
5 Prestera, T., Holtzclaw, W. D., Zhang, Y. and Talalay, P. (1993) Chemical and molecular regulation of enzymes that detoxify carcinogens. Proc. Natl. Acad. Sci. U.S.A. **90**, 2965–2969
6 Dinkova-Kostova, A. T., Massiah, M. A., Bozak, R. E., Hicks, R. J. and Talalay, P. (2001) Potency of Michael reaction acceptors as inducers of enzymes that protect against carcinogenesis depends on their reactivity with sulfhydryl groups. Proc. Natl. Acad. Sci. U.S.A. **98**, 3404–3409
7 Hayes, J. D., Chanas, S. A., Henderson, C. J., McMahon, M., Sun, C., Moffat, G. J., Wolf, C. R. and Yamamoto, M. (2000) The Nrf2 transcription factor contributes both to the basal expression of glutathione S-transferases in mouse liver and to their induction by the chemopreventive synthetic antioxidants, butylated hydroxyanisole and ethoxyquin. Biochem. Soc. Trans. **28**, 33–41
8 Venugopal, R. and Jaiswal, A. K. (1996) Nrf1 and Nrf2 positively and c-Fos and Fra1 negatively regulate the human antioxidant response element-mediated expression of NAD(P)H:quinone oxidoreductase$_1$ gene. Proc. Natl. Acad. Sci. U.S.A. **93**, 14960–14965
9 Itoh, K., Chiba, T., Takahashi, S., Ishii, T., Igarashi, K., Katoh, Y., Oyake, T., Hayashi, N., Satoh, K., Hatayama, I. et al. (1997) An Nrf2/small Maf heterodimer mediates the induction of phase II detoxifying enzyme genes through antioxidant response elements. Biochem. Biophys. Res. Commun. **236**, 313–322
10 Zhu, M. and Fahl, W. E. (2001) Functional characterization of transcription regulators that interact with the electrophile response element. Biochem. Biophys. Res. Commun. **289**, 212–219
11 Hayes, J. D. and McMahon, M. (2001) Molecular basis for the contribution of the antioxidant responsive element to cancer chemoprevention. Cancer Lett. **174**, 103–113
12 Ishii, T., Itoh, K., Takahashi, S., Sato, H., Yanagawa, T., Katoh, Y., Bannai, S. and Yamamoto, M. (2000) Transcription factor Nrf2 coordinately regulates a group of oxidative stress-inducible genes in macrophages. J. Biol. Chem. **275**, 16023–16029
13 Enomoto, A., Itoh, K., Nagayoshi, E., Haruta, J., Kimura, T., O'Connor, T., Harada, T. and Yamamoto, M. (2001) High sensitivity of Nrf2 knockout mice to acetaminophen hepatotoxicity associated with decreased expression of ARE-regulated drug metabolizing enzymes and antioxidant genes. Toxicol. Sci. **59**, 169–177
14 Chan, K., Han, X.-D. and Kan, Y. W. (2001) An important function of Nrf2 in combating oxidative stress: detoxification of acetaminophen. Proc. Natl. Acad. Sci. U.S.A. **98**, 4611–4616
15 Chan, K. and Kan, Y. W. (1999) Nrf2 is essential for protection against acute pulmonary injury in mice. Proc. Natl. Acad. Sci. U.S.A. **96**, 12731–12736
16 McMahon, M., Itoh, K., Yamamoto, M., Chanas, S. A., Henderson, C. J., McLellan, L. I., Wolf, C. R., Cavin, C. and Hayes, J. D. (2001) The cap'n'collar basic leucine zipper transcription factor Nrf2 (NF-E2 p45-related factor 2) controls both constitutive and inducible expression of intestinal detoxification and glutathione biosynthetic enzymes. Cancer Res. **61**, 3299–3307
17 Aoki, Y., Sato, H., Nishimura, N., Takahashi, S., Itoh, K. and Yamamoto, M. (2001) Accelerated DNA adduct formation in the lung of the Nrf2 knockout mouse exposed to diesel exhaust. Toxicol. Appl. Pharmacol. **173**, 154–160
18 Ramos-Gomez, M., Kwak, M.-K., Dolan, P. M., Itoh, K., Yamamoto, M., Talalay, P. and Kensler, T. W. (2001) Sensitivity to carcinogenesis is increased and chemoprotective efficacy of enzyme inducers is lost in *nrf2* transcription factor-deficient mice. Proc. Natl. Acad. Sci. U.S.A. **98**, 3410–3415
19 Cho, H.-Y., Jedlicka, A. E., Reddy, S. P. M., Zhang, L.-Y., Kensler, T. W. and Kleeberger, S. R. (2002) Linkage analysis of susceptibility to hyperoxia: Nrf2 is a candidate gene. Am. J. Respir. Cell. Mol. Biol. **26**, 42–51
20 Morimitsu, Y., Nakagawa, Y., Hayashi, K., Fujii, H., Kumagai, T., Nakamura, Y., Osawa, T., Horio, F., Itoh, K., Iida, K. et al. (2002) A sulforaphane analogue that potently activates the Nrf2-dependent detoxification pathway. J. Biol. Chem. **277**, 3456–3463
21 Friling, R. S., Bensimon, A., Tichauer, Y. and Daniel, V. (1990) Xenobiotic-inducible expression of murine glutathione S-transferase Ya subunit gene is controlled by an electrophile-responsive element. Proc. Natl. Acad. Sci. U.S.A. **87**, 6258–6262

22 Hayes, J. D., Kerr, L. A., Peacock, S. D., Cronshaw, A. D. and McLellan, L. I. (1991) Hepatic glutathione *S*-transferases in mice fed on a diet containing the anticarcinogenic antioxidant butylated hydroxyanisole. Isolation of mouse glutathione *S*-transferase heterodimers by gradient elution of the glutathione–Sepharose affinity matrix. Biochem. J. **277**, 501–512
23 Hayes, J. D. and Pulford, D. J. (1995) The glutathione S-transferase supergene family: regulation of GST and the contribution of the isoenzymes to cancer chemoprotection and drug resistance. Crit. Rev. Biochem. Mol. Biol. **30**, 445–600
24 Pearson, W. R., Reinhart, J., Sisk, S. C., Anderson, K. S. and Adler, P. N. (1988) Tissue-specific induction of murine glutathione transferase mRNAs by butylated hydroxyanisole. J. Biol. Chem. **263**, 13324–13332
25 Townsend, A. J., Goldsmith, M. E., Pickett, C. B. and Cowan, K. H. (1989) Isolation, characterization, and expression in *Escherichia coli* of two murine Mu class glutathione *S*-transferase cDNAs homologous to the rat subunits 3 (Yb1) and 4 (Yb2). J. Biol. Chem. **264**, 21582–21590
26 Fulcher, K. D., Welch, J. E., Klapper, D. G., O'Brien, D. A. and Eddy, E. M. (1995) Identification of a unique μ-class glutathione S-transferase in mouse spermatogenic cells. Mol. Reprod. Dev. **42**, 415–424
27 Rowe, J. D., Patskovsky, Y. V., Patskovska, L. N., Novikova, E. and Listowsky, I. (1998) Rationale for reclassification of a distinctive subdivision of mammalian class Mu glutathione *S*-transferases that are primarily expressed in testis. J. Biol. Chem. **273**, 9593–9601
28 De Bruin, W. C. C., Te Morsche, R. H. M., Wagenmans, M. J. M., Alferink, J. C., Townsend, A. J., Wieringa, B. and Peters, W. H. M. (1998) Identification of a novel murine glutathione *S*-transferase class mu gene. Biochem. J. **330**, 623–626
29 Johnson, J. A., Finn, K. A. and Siegel, F. L. (1992) Tissue distribution of enzymic methylation of glutathione *S*-transferase and its effects on catalytic activity. Methylation of glutathione *S*-transferase 11-11 inhibits conjugating activity towards 1-chloro-2,4-dinitrobenzene. Biochem. J. **282**, 279–289
30 McLellan, L. I., Kerr, L. A., Cronshaw, A. D. and Hayes, J. D. (1991) Regulation of mouse glutathione *S*-transferases by chemoprotectors. Molecular evidence for the existence of three distinct Alpha-class glutathione *S*-transferase subunits, Ya_1, Ya_2 and Ya_3, in mouse liver. Biochem. J. **276**, 461–469
31 Mitchell, A. E., Morin, D., Lakritz, J. and Jones, A. D. (1997) Quantitative profiling of tissue- and gender-related expression of glutathione *S*-transferase isoenzymes in the mouse. Biochem. J. **325**, 207–216
32 McLellan, L. I. and Hayes, J. D. (1987) Sex-specific constitutive expression of the pre-neoplastic marker glutathione *S*-transferase, YfYf, in mouse liver. Biochem. J. **245**, 399–406
33 McLellan, L. I., Harrison, D. J. and Hayes, J. D. (1992) Modulation of glutathione S-transferases and glutathione peroxidase by the anticarcinogen butylated hydroxyanisole in murine extrahepatic organs. Carcinogenesis **13**, 2255–2261
34 McLellan, L. I. and Hayes, J. D. (1989) Differential induction of class Alpha glutathione *S*-transferases in mouse liver by the anticarcinogenic antioxidant, butylated hydroxyanisole. Biochem. J. **263**, 393–402
35 Hu, X., Benson, P. J., Srivastava, S. K., Mack, L. M., Xia, H., Gupta, V., Zaren, H. A. and Singh, S. V. (1996) Glutathione *S*-transferases of female A/J mouse liver and forestomach and their differential induction by anti-carcinogenic organosulfides from garlic. Arch. Biochem. Biophys. **336**, 199–214
36 Hu, X., Srivastava, S. K., Xia, H., Awasthi, Y. C. and Singh, S. V. (1996) An alpha class mouse glutathione *S*-transferase with exceptional catalytic efficiency in the conjugation of glutathione with 7β,8α-dihydroxy-9α,10α-oxy-7,8,9,10-tetrahydrobenzo(*a*)pyrene. J. Biol. Chem. **271**, 32684–32688
37 Hu, X., Seidel, A., Frank, H., Srivastava, S. K., Xia, H., Pal, A., Zheng, S., Oesch, F. and Singh, S. V. (1998) Differential enantioselectivity of murine glutathione *S*-transferase isoenzymes in the glutathione conjugation of *trans*-3,4-dihydroxy-1,2-oxy-1,2,3,4-tetrahydrobenzo[*c*]phenanthrene stereoisomers. Arch. Biochem. Biophys. **358**, 40–48
38 Hayes, J. D., Judah, D. J., Neal, G. E. and Nguyen, T. (1992) Molecular cloning and heterologous expression of a cDNA encoding a mouse glutathione S-transferase Yc subunit possessing high catalytic activity for aflatoxin B_1-8,9-epoxide. Biochem. J. **285**, 173–180
39 Buetler, T. M., Slone, D. and Eaton, D. L. (1992) Comparison of the aflatoxin B_1-8,9-epoxide conjugating activities of two bacterially expressed Alpha class glutathione S-transferase isozymes from mouse and rat. Biochem. Biophys. Res. Commun. **188**, 597–603
40 Townsend, A. J., Fields, W. R., Haynes, R. L., Doss, A. J., Li, Y., Doehmer, J. and Morrow, C. S. (1998) Chemoprotective functions of glutathione S-transferases in cell lines induced to express specific isoenzymes by stable transfection. Chem. Biol. Interact. **112**, 389–407
41 Kwak, M.-K., Egner, P. A., Dolan, P. M., Ramos-Gomez, M., Groopman, J. D., Itoh, K., Yamamoto, M. and Kensler, T. W. (2001) Role of phase 2 enzyme induction in chemoprotection by dithiolethiones. Mutat. Res. **480**, 305–315
42 Reinhart, J. and Pearson, W. R. (1993) The structure of two murine class-Mu glutathione transferase genes coordinately induced by butylated hydroxyanisole. Arch. Biochem. Biophys. **303**, 383–393
43 Favreau, L. V. and Pickett, C. B. (1995) The rat quinone reductase antioxidant response element. Identification of the nucleotide sequence required for basal and inducible activity and detection of antioxidant response element-binding proteins in hepatoma and non-hepatoma cell lines. J. Biol. Chem. **270**, 24468–24474
44 Nguyen, T., Huang, H. C. and Pickett, C. B. (2000) Transcriptional regulation of the antioxidant response element. Activation by Nrf2 and repression by MafK. J. Biol. Chem. **275**, 15466–15473
45 Sisk, S. C. and Pearson, W. R. (1993) Differences in induction by xenobiotics in murine tissues and the Hepa1c1c7 cell line of mRNAs encoding glutathione transferase, quinone reductase, and CYP1A P450s. Pharmacogenetics **3**, 167–181
46 Yoshioka, K., Deng, T., Cavigelli, M. and Karin, M. (1995) Antitumor promotion by phenolic antioxidants: inhibition of AP-1 activity through induction of Fra expression. Proc. Natl. Acad. Sci. U.S.A. **92**, 4972–4976
47 He, C. H., Gong, P., Hu, B., Stewart, D., Choi, M. E., Choi, A. M. K. and Alam, J. (2001) Identification of activating transcription factor 4 (ATF4) as an Nrf2-interacting protein. Implications for heme oxygenase-1 gene regulation. J. Biol. Chem. **276**, 20858–20865
48 Bammler, T. K., Smith, C. A. D. and Wolf, C. R. (1994) Isolation and characterization of two mouse Pi-class glutathione S-transferase genes. Biochem. J. **298**, 385–390
49 Xu, X. and Stambrook, P. J. (1994) Two murine GSTpi genes are arranged in tandem and are differently expressed. J. Biol. Chem. **269**, 30268–30273
50 Peters, M. M. C. G., Lau, S. S., Dulik, D., Murphy, D., van Ommen, B., van Bladeren, P. J. and Monks, T. J. (1996) Metabolism of *tert*-butylhydroquinone to *S*-substituted conjugates in the male Fischer 344 rat. Chem. Res. Toxicol. **9**, 133–139

Received 25 February 2002/16 April 2002; accepted 3 May 2002
Published as BJ Immediate Publication 3 May 2002, DOI 10.1042/BJ2002/0320

MOLECULAR AND CELLULAR BIOLOGY, Feb. 2003, p. 1163–1174 Vol. 23, No. 4
0270-7306/03/$08.00+0 DOI: 10.1128/MCB.23.4.1163–1174.2003

Small Maf Compound Mutants Display Central Nervous System Neuronal Degeneration, Aberrant Transcription, and Bach Protein Mislocalization Coincident with Myoclonus and Abnormal Startle Response

Fumiki Katsuoka,[1,2] Hozumi Motohashi,[1,2] Yuna Tamagawa,[1] Shigeo Kure,[3] Kazuhiko Igarashi,[4] James Douglas Engel,[2]* and Masayuki Yamamoto[1]*

Institute of Basic Medical Sciences and Center for Tsukuba Advanced Research Alliance, University of Tsukuba, Tsukuba 305-8577,[1] Department of Medical Genetics, Tohoku University School of Medicine, Sendai 980-8574,[3] and Department of Biomedical Chemistry, Graduate School of Biomedical Sciences, Hiroshima University, Hiroshima 734-8551,[4] Japan, and Department of Cell and Developmental Biology and Center for Organogenesis, University of Michigan, Ann Arbor, Michigan 48109-0616[2]

Received 5 August 2002/Returned for modification 24 September 2002/Accepted 7 November 2002

The small Maf proteins form heterodimers with CNC and Bach family proteins to elicit transcriptional responses from Maf recognition elements (MAREs). We previously reported germ line-targeted deficiencies in *mafG* plus *mafK* compound mutant mice. The most prominent mutant phenotype was a progressive *maf* dosage-dependent neuromuscular dysfunction. However, there has been no previous report regarding the effects of altered small-*maf* gene expression on neurological dysfunction. We show here that MafG and MafK are expressed in discrete central nervous system (CNS) neurons and that *mafG::mafK* compound mutants display neuronal degeneration coincident with surprisingly selective MARE-dependent transcriptional abnormalities. The CNS morphological changes are concurrent with the onset of a neurological disorder in the mutants, and the behavioral changes are accompanied by reduced glycine receptor subunit accumulation. Bach/small Maf heterodimers, which normally generate transcriptional repressors, were significantly underrepresented in nuclear extracts prepared from *maf* mutant brains, and Bach proteins fail to accumulate normally in nuclei. Thus compound *mafG::mafK* mutants develop age- and *maf* gene dosage-dependent cell-autonomous neuronal deficiencies that lead to profound neurological defects.

The small Maf proteins were originally identified by their strong homology to the transforming v-Maf oncoprotein of avian retrovirus AS42 (16). Three members constitute the small Maf family, MafF, MafG, and MafK, but no differences between them have been revealed in functional studies (14). All three small Maf proteins possess a basic region-leucine zipper (bZip) motif that mediates DNA binding and dimer formation; however, they lack any recognizable transcriptional effector domain. The small Maf proteins can form homodimers or heterodimers among themselves, and they can also heterodimerize with other bZip transcription factors, including CNC proteins, Bach proteins, and Fos family members, and thus can bind to Maf recognition elements (MAREs) in DNA (24, 25). Large Maf proteins and AP-1 family members also bind to MAREs, as the extended MARE sequence also contains an internal tetradecanoyl phorbol acetate-responsive element (24, 25). All of these factors have the potential to participate in transcriptional regulation through MAREs in the promoters and enhancers of many different genes, most prominently in the hematopoietic system but also in key phase II detoxifying-enzyme genes (11, 24).

One powerful approach to glean insight into the functional roles of specific gene products is through loss-of-function analysis. To date, three of the four *CNC* genes have been disrupted by gene targeting, and conspicuous phenotypes have been reported. For example, *p45 NF-E2*-null mutant mice are severely thrombocytopenic and therefore defective in megakaryopoiesis and platelet production (33). *nrf1*-null mutant mice die during gestation of a non-cell-autonomous anemia (5). *nrf2*-null mutant mice are viable but have severely impaired antioxidant and phase II detoxification enzyme gene responses (11).

The small Maf proteins are obligatory partner molecules of CNC and Bach family proteins in generating both repressing and activating transcriptional activities. The small Maf proteins are expressed in broadly overlapping, but individually distinct, patterns (27), and their expression changes dynamically during embryonic development (9, 15, 22). These observations suggested that small Maf abundance in any given tissue could be critical for MARE-dependent gene regulation. However, no apparent phenotype was detected in either *mafK*- or *mafF*-null mutant mice (19, 27, 31). In contrast, *mafG* mutant mice displayed both mild neurological and hematological phenotypes (31). Because of their partially overlapping embryonic expression profiles and apparently identical biochemical characteristics, we suspected that the small Maf proteins might be par-

* Corresponding author. Mailing address for James Douglas Engel: Department of Cell and Developmental Biology and Center for Organogenesis, University of Michigan Medical School, Ann Arbor, MI 48109-0616. Phone: (734) 615-7509. Fax: (734) 763-1166. E-mail: engel@umich.edu. Mailing address for Masayuki Yamamoto: Institute of Basic Medical Sciences and Center for Tsukuba Advanced Research Alliance, University of Tsukuba, Tsukuba 305-8577, Japan. Phone: 81-298-53-6158. Fax: 81-298-53-7318. E-mail: masi@tara.tsukuba.ac.jp.

tially or completely redundant for any single disruption in gene function.

After combining the *maf* mutations, we discovered that the *mafG*::*mafK* compound mutants displayed far more severe phenotypes than did mutants with the *mafG* mutation alone: thrombocytopenia was exacerbated (thus phenocopying the *p45 NF-E2* mutation) (33), while the neurological phenotype presented much earlier in development (28). Only a fraction of $mafG^{-/-}$ mutant mice displayed hind leg clasping, a mild motor dysfunction, with initial onset at about 6 months of age (31). In contrast, $mafG^{-/-}$::$mafK^{+/-}$ (bearing one active *mafK* allele) mice displayed a more severe neuromuscular disorder, with a far earlier onset in all of the mice. Neither $mafG^{+/-}$::$mafK^{+/-}$ nor $mafG^{+/-}$::$mafK^{-/-}$ mice displayed a significant phenotype (28). Therefore, based on the severity of these phenotypes, the genotypes of the compound *maf* mutant mice could be ordered by rank: rank 1 (essentially unaffected mice), $mafK^{-/-}$, $mafG^{+/-}$::$mafK^{+/-}$, and $mafG^{+/-}$::$mafK^{-/-}$; rank 2 (mice with mild adult onset), $mafG^{-/-}$; rank 3 (mice with severe pubertal onset), $mafG^{-/-}$::$mafK^{+/-}$; rank 4 (mice that died at weaning), $mafG^{-/-}$::$mafK^{-/-}$. When we analyzed the expression of all three small *maf* genes in a spectrum of different tissues by RNase protection and quantitative PCR, we found that nearly 90% of total small *maf* mRNA expressed in the brain was derived from *mafG* (28). Consequently, the phenotypic severity is what might have been predicted from the small Maf expression abundances. These results implied that gene dosage (and thus the total small Maf concentration) might be an important underlying cause of the neurological disorder and thus that small Maf proteins might act upstream in a motor pathway that normally regulates an unknown, but critical, behavioral determinant(s).

In support of this "Maf dosage" hypothesis, we recently reported that small-Maf protein abundance is crucial for MARE-dependent regulation of the terminal stages of megakaryopoiesis (23). However, since the *mafG* mutants, but not any *CNC* gene mutants, additionally exhibited a neurological phenotype, we exploited this unique, dosage-dependent characteristic of the small *maf* gene loss-of-function mutations to explore the molecular mechanisms underlying the neurological disorder.

We first examined tissues histologically to identify changes in neural tissue(s) that correlated with the progressive motor disease. We found that pathological changes initiated after birth and were widespread in neurons of the central nervous system (CNS) but not in glial cells. The *maf* mutant mice displayed a hypertonic motor disorder and abnormal responses to startle stimuli. In exploring similarities between the *maf* mutants and mice with spontaneous neurological mutations that have been reported in the literature, we discovered that mice bearing mutant glycine receptors also exhibited abnormal startle responses (17, 18, 30). In keeping with the hypothesis that the pathways leading to the similar phenotypes might intersect, we found that the abundance of the glycine receptor α 1 (Glra1) subunit is reduced in symptomatic *maf* mutant mice and that the progression of neurological changes in the *maf* mutants begins postnatally at 3 weeks, coincident temporally with *Glra1* gene transcriptional induction in wild-type mice. Although we anticipated that antioxidant genes in the CNS that are normally regulated through MAREs would be repressed in the mutants, we observed instead only selective induction of MARE-dependent antioxidant genes. We found that CNS MARE-binding proteins, comprising in part Bach/small Maf heterodimers, were diminished in symptomatic mutant animals and that nuclear accumulation of the Bach proteins was severely impaired. We conclude from these data that compound $mafG^{-/-}$::$mafK^{+/-}$ mutant mice display cell-autonomous neuronal abnormalities that are accompanied by misregulated neuronal MARE-binding activity and that one element of the complex neuropathology exhibited by these mice may be due to a glycine receptor deficiency. Thus the small Maf proteins play a critical role in the maintenance of normal CNS function, as they do in megakaryopoiesis.

MATERIALS AND METHODS

Behavioral studies. A cohort of 31 $mafG^{+/-}$::$mafK^{+/-}$ mice and 30 $mafG^{-/-}$::$mafK^{+/-}$ mice were tested at 3, 6, and 9 weeks of age to determine the time of onset and penetrance of the neurological phenotype. When a mouse was held by the tail and displayed hind limb clasping (see Fig. 1A) within 1 min, it was scored as positive. When a mouse was put on the table and myoclonus was triggered in limb extremities at least once within a minute, this mouse was judged to display myoclonus.

Eight- to 11-week-old mice were used for testing acoustic responses. The MRC Institution of Hearing Research click box generates a brief 18- to 20-kHz tone at 94 dB sound pressure level. For measuring locomotor activity, an empty plastic cage was used and locomotion was recorded by SUPERMEX (Muromachi Kikai Co.). Ambulation was scored by using a personal computer interfaced to a mouse body temperature-sensitive sensor (6, 20). To evaluate diminished locomotor activity after acoustic stimuli, we adopted the value of the mean locomotor activity for 2 min after a stimulus divided by the activity for the 5 min preceding the stimulus. Five mice of each genotype were tested, and acoustic stimuli were generated sequentially three times, separated by 10-min intervals.

LacZ activity. Mouse brains were fixed in 1% formaldehyde–0.2% glutaraldehyde–0.02% NP-40 in phosphate-buffered saline and embedded in OCT compound (Tissue-Tek; Sakura). Sections were stained with X-Gal (5-bromo-4-chloro-3-indolyl-β-D-galactopyranoside) solution as previously described (15). Nuclear fast red was used for counterstaining.

Histological analyses. Mouse tissues were fixed in 3.7% formaldehyde and embedded in paraffin. For Nissl staining, the paraffin was removed prior to cresyl violet staining. For ubiquitin immunostaining, sections were processed for immunohistochemistry with the ABC horseradish peroxidase kit (Vector Laboratory) after paraffin removal. The ubiquitin antibody (Santa Cruz Biotechnology) was diluted to 1:200, diaminobenzidine was used as the substrate for chromogen development, and methyl green was used for counterstaining.

In situ hybridization. Mouse brain stems were fixed in 4% paraformaldehyde-phosphate-buffered saline and embedded in paraffin. In situ hybridizations were carried out with a digoxigenin-alkaline phosphatase system (Roche). The *HO-1* cDNA in pBluescript was a generous gift from T. Ishii (University of Tsukuba) and was used to generate RNA probes. Hybridization was performed as previously described (22).

RNA blots. Total RNA was prepared by using Isogen (Nippon Gene). RNA was electrophoresed on a formaldehyde-agarose gel and transferred to a nylon membrane. ^{32}P-labeled probes were prepared from the same *HO-1* cDNA that was used for in situ hybridization, *Gbx1* and *Glrb* cDNAs were generated by PCR, and NMDAR1 was a generous gift from S. Nakanishi (Kyoto University).

Electrophoretic mobility shift assay (EMSA). Brain nuclear extracts were prepared as described previously (4). Double-stranded MARE oligonucleotide probe no. 25 (14) was radiolabeled with ^{32}P, and incubation of the probe and nuclear extracts was carried out as described previously (14). The protein-DNA complexes and free probe were resolved by electrophoresis on a 5% polyacrylamide gel in 1× Tris-borate-EDTA buffer. An anti-Bach antibody (F69-1 [29]) and an anti-small Maf antibody (8) were used as originally described.

Western blots. For the detection of Bach proteins, 10 μg of nuclear extract or whole-cell extract was separated by sodium dodecyl sulfate-polyacrylamide gel electrophoresis and then transferred to a polyvinylidene difluoride membrane. Expression of Bach and Nrf1 proteins was examined with the anti-pan-Bach antibody (F69-1) and an anti-Nrf1 antibody (Santa Cruz Biotechnology), respectively. For the detection of the Glra1 subunit, whole-cell extracts were prepared from brain stems of 7-month-old mice. Thirty micrograms of protein was used

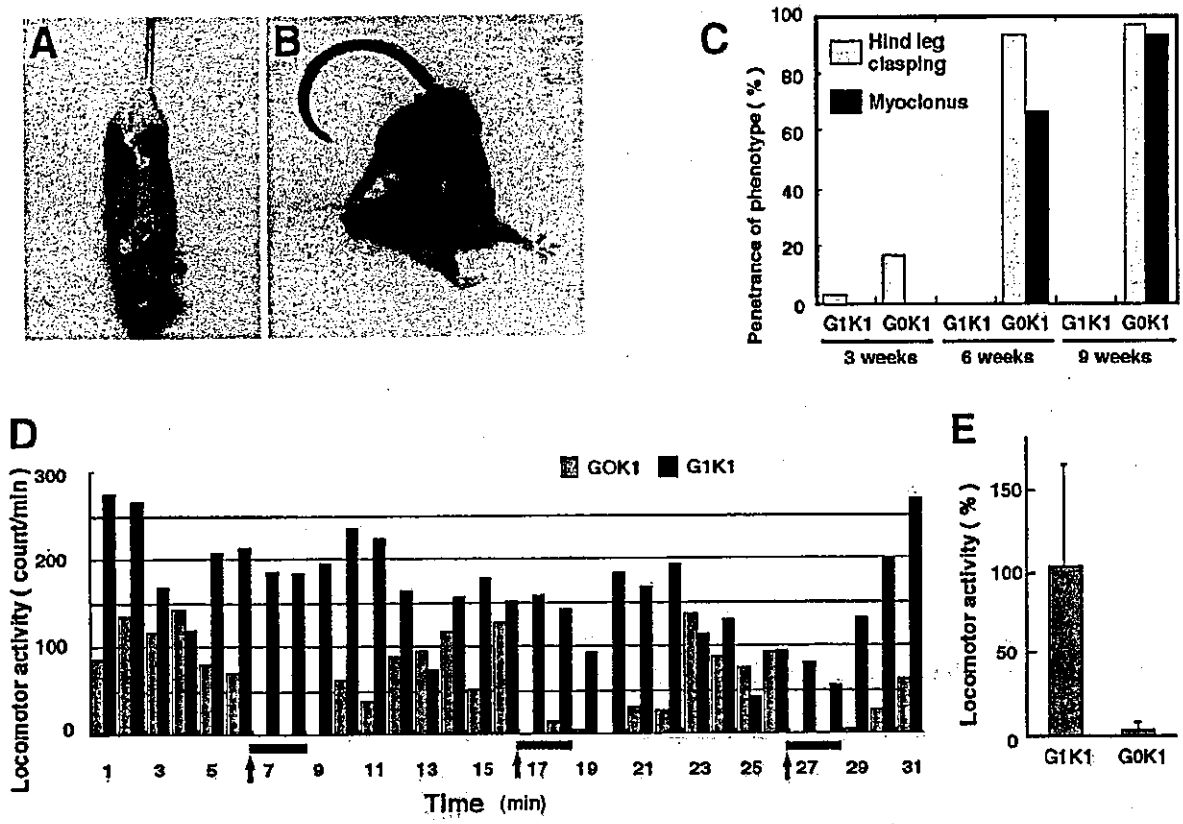

FIG. 1. Behavioral analysis of *mafG::mafK* compound mutant mice. (A) A *mafG*$^{-/-}$::*mafK*$^{+/-}$ mutant mouse (6 weeks old) displaying characteristic hind leg clasping. (B) A *mafG*$^{-/-}$::*mafK*$^{+/-}$ mutant mouse (10 weeks) with long-lasting myoclonus. (C) The penetrance of the motor disorder was examined at 3, 6, and 9 weeks of age. Bars indicate frequencies of mice displaying each phenotype. G1K1 and G0K1, *mafG*$^{+/-}$::*mafK*$^{+/-}$ control and *mafG*$^{-/-}$::*mafK*$^{+/-}$ mutant, respectively. (D) Representative pattern of locomotor activities of *mafG*$^{-/-}$::*mafK*$^{+/-}$ (mutant) and *mafG*$^{+/-}$::*mafK*$^{+/-}$ (control) mice. Each bar indicates the frequency of ambulation per minute. Arrows, times of acoustic stimuli. (E) Comparison of the influences of acoustic stimuli on the locomotor activities of mutant and control mice. The mean ambulation count for 2 min after stimulus (red bars in panel D) was divided by that for 5 min before stimulus. This value was averaged for five independent animals and depicted as a bar. Error bars, standard deviations.

per sample lane. The antibody recognizing the Glra1 subunit was purchased from Calbiochem.

Transfection and immunostaining. pCMV/Bach1 and pCMV/Bach2 were used for forced expression of Bach1 and Bach2, respectively (29). pIM-MafK and pIM-MafKL2PM4P were used for transient expression of MafK and a MafK leucine zipper-defective mutant (MafKL2PM4P), respectively (23). These expression vectors were transfected into NIH 3T3 cells with FuGENE6 (Roche). At 24 h after transfection, cells were fixed with methanol at −20°C for 5 min and treated with 0.1% Triton X-100. After being blocked with 2% goat serum, cells were reacted with the anti-Bach1 antibody for 1 h and then with fluorescein isothiocyanate-conjugated anti-rabbit immunoglobulin G. After the secondary-antibody solution was washed away, cell nuclei were stained with DAPI (4′,6′-diamidino-2-phenylindole). One hundred transfected cells were examined and classified into three categories: C>N (predominantly cytoplasmic staining); C=N (a roughly equal distribution between cytoplasmic and nuclear compartments), and C<N (predominantly nuclear staining).

RESULTS

***mafG*$^{-/-}$::*mafK*$^{+/-}$ mice display a progressive motor disorder.** The neurological phenotype in *mafG* null mutant mice was detectable only after approximately 6 months of age and was incompletely penetrant (31). The same (but fully penetrant) phenotype appeared earliest in *mafG*$^{-/-}$::*mafK*$^{-/-}$ (compound null) mutant mice, but these animals survived only to about 3 weeks of age (28). We therefore chose to subject *mafG*$^{-/-}$::*mafK*$^{+/-}$ compound mutants, bearing one active *mafK* allele, to detailed scrutiny since they had an almost normal life span and yet the neurological phenotype occurred early and was fully penetrant. For this analysis we compared the neurological phenotypes of the *mafG*$^{-/-}$::*mafK*$^{+/-}$ mice to those of the *mafG*$^{+/-}$::*mafK*$^{+/-}$ control littermates (mutant for one allele of both *mafK* and *mafG*), which display no neurological phenotype.

More than one-half of the *mafG*$^{-/-}$::*mafK*$^{+/-}$ mutant mice developed a characteristic hind leg clasping by the sixth week after birth (Fig. 1A and C). Two-thirds of the mutant mice began to show intermittent and long-lasting hind limb or tetrapodic myoclonus (Fig. 1B), and this aberrant behavior was fully penetrant by 9 weeks of age (Fig. 1C). None of the *mafG*$^{+/-}$::*mafK*$^{+/-}$ (Fig. 1C) control mice were affected.

Myoclonus occurred spontaneously in the mutant mice but could also be triggered by external stimuli. By monitoring the nocturnal behavior of the mutant mice, we discovered that the hind leg myoclonus was triggered when the mutant mice began to eat with their forepaws. Myoclonus was also observed when

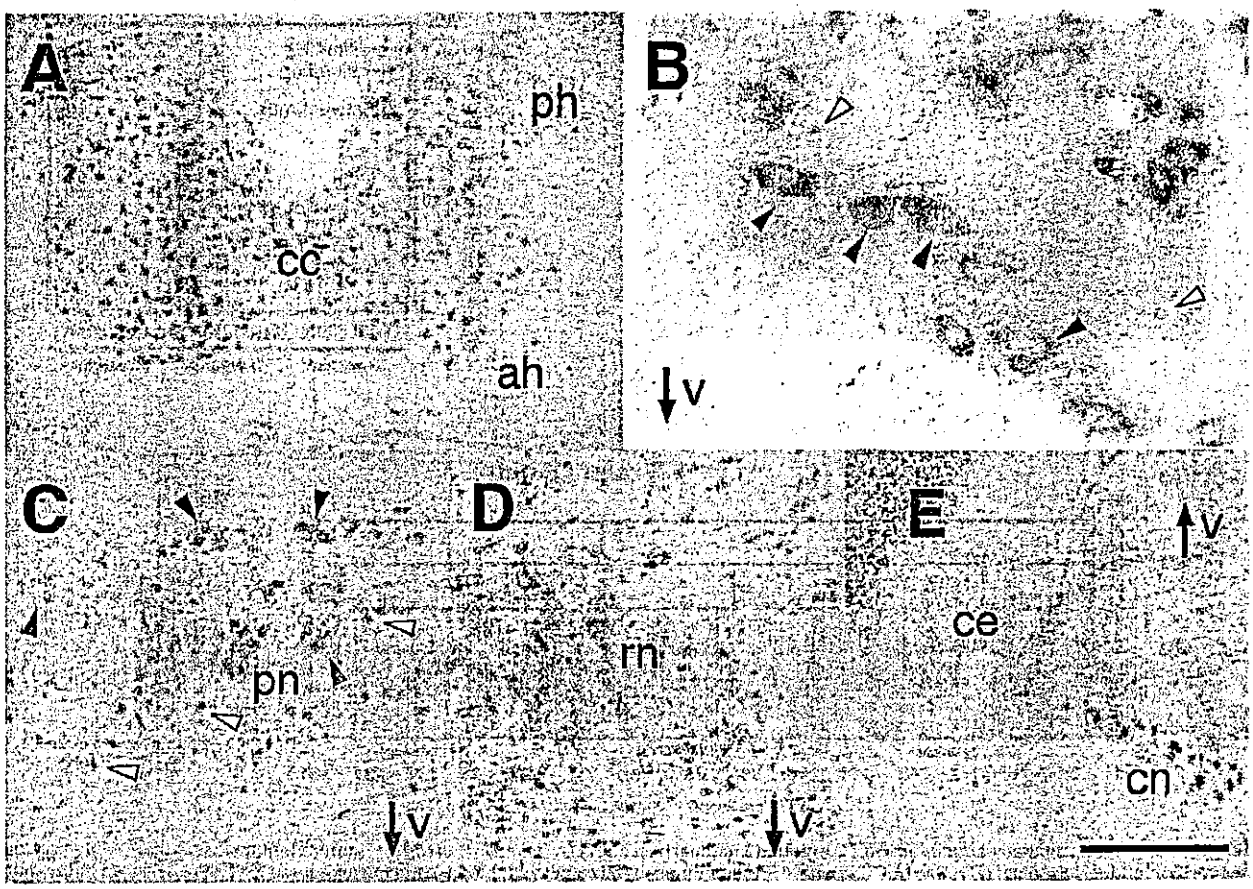

FIG. 2. *mafG* gene expression in the CNS. Tissue sections from a *mafG*$^{+/-}$ mouse were prepared and stained for β-galactosidase activity. LacZ activity (blue) was observed exclusively in neurons (not in glial cells) in the spinal cord (A and B), pons (C), medulla (D), and cerebellar nuclei (E). Solid arrowheads, neurons; open arrowheads, glia; arrows beside V, ventral side. Scale bar, 450 (A and E), 90 (B), 110 (C), or 150 μm (D). cc, central canal; ah, anterior horn; ph, posterior horn; pn, pontine nuclei; rn, reticular nuclei; cn, cerebellar nuclei; ce, cerebellum.

the mutants approached the edge of a table during free locomotion, behavior that seemed to be triggered by visual stimuli (data not shown).

Anticipating that this neurological deficiency might originate in the CNS (see below), we monitored the locomotor activity of *mafG*$^{-/-}$::*mafK*$^{+/-}$ mutant mice in response to acoustic stimuli, and Fig. 1D shows a representative pattern of activity before and after stimulation. The activity of *mafG*$^{-/-}$::*mafK*$^{+/-}$ mutant mice was quantifiably repressed after stimulation, while *mafG*$^{+/-}$::*mafK*$^{+/-}$ control littermates displayed little response. Five mice of each genotype were examined, and the average locomotor activities for 2 min following the acoustic stimulus were compared. The data depict a qualitative difference in acoustic response between *mafG*$^{+/-}$::*mafK*$^{+/-}$ control and *mafG*$^{-/-}$::*mafK*$^{+/-}$ mutant mice (Fig. 1E).

MafG and MafK are both expressed in neurons. We previously reported that MafK is widely expressed in neurons, but not in glial cells, of the CNS. The large cells morphologically identified as neurons generally express MafK mRNA in the spinal cord, brain stem, hippocampus, and dorsal root ganglia (22). To ask whether diminished MafK and MafG expression might lead to exclusively neuronal deficiencies, we examined *mafG* expression in the CNS by monitoring the expression of the *lacZ* gene, which was used to replace the coding sequences of *mafG* during the generation of the targeted mutant mice (31). β-Galactosidase activity was observed primarily in neurons, but not in glia, of the spinal cord (Fig. 2A and B); this was also true in the brain stem (Fig. 2C to E) and hippocampus and dorsal root ganglia (data not shown). Especially in spinal cord gray matter and cerebellar nuclei, almost all the recognizable neurons expressed MafG (Fig. 2A and E) as well as MafK (22), indicating overlapping expression of the two genes. The data show that MafG and MafK are predominantly, if not exclusively, expressed in neurons in the CNS.

CNS neuronal degeneration in *mafG*$^{-/-}$::*mafK*$^{+/-}$ mice. To investigate the underlying cellular basis for the observed neuronal disorder, we performed histological examination of neural tissues from 10-week-old *mafG*$^{-/-}$::*mafK*$^{+/-}$ mice that displayed pathological behavior. The numbers of Nissl-staining neurons in the gray matter of the spinal cord in *mafG*$^{-/-}$::*mafK*$^{+/-}$ mutant mice and *mafG*$^{+/-}$::*mafK*$^{+/-}$ controls appeared to be almost the same, albeit with slightly weaker staining in the mutants (Fig. 3A and B). When the same sections were examined at higher magnification, however, a conspicuous difference between the two genotypes was consistently observed. Many of the neuronal nuclei in the affected mouse

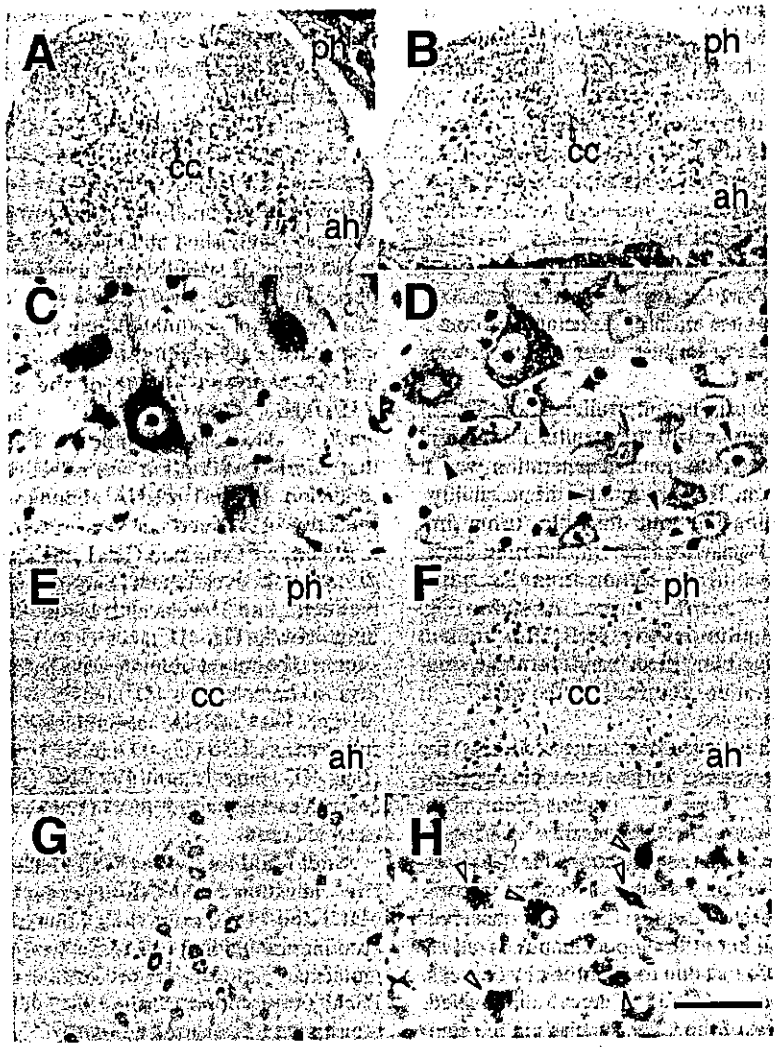

FIG. 3. Histopathological changes in CNS neurons of *maf* mutant mice. (A to D) Nissl staining of spinal cord sections from 10-week-old *mafG*$^{+/-}$::*mafK*$^{+/-}$ control mice (A and C) and *mafG*$^{-/-}$::*mafK*$^{+/-}$ mutant mice (B and D) displaying myoclonus. Solid arrowheads (D), swollen nuclei with minimal cytoplasm in the affected mice. (E to G) Immunostaining for ubiquitin in spinal cord sections from control *mafG*$^{+/-}$::*mafK*$^{+/-}$ mice (E) and *mafG*$^{-/-}$::*mafK*$^{+/-}$ mutant mice (F and G). The mutants display far more intense staining, primarily in neuronal nuclei (G). (H) Double staining for β-galactosidase activity and ubiquitin immunohistological activity on brain stem sections prepared from 4-week-old *mafG*$^{-/-}$::*mafK*$^{+/-}$ mutant mice. Note that all the cells in which ubiquitin has accumulated (intense brown signal) are also LacZ positive (open arrowheads). Scale bar, 400 (A, B, E, and F), 40 (C and D), 120 (G), or 60 μm (H). Abbreviations are as defined in the legend to Fig. 2.

spinal cord were swollen, and their cytoplasm was thin, containing few Nissl bodies (Fig. 3C and D). The neurons in the anterolateral column of the spinal cord were less severely affected but still contained fewer Nissl bodies than controls. The same morphological characteristics were observed along the entire length of the spinal cord and brain stem. Similarly affected neurons were also distributed throughout the thalamus, hippocampus, and cerebral cortex (data not shown). These same cellular changes were not detected in the comparable tissues of 1-week-old mutants but became apparent even as early as 3 weeks of age (before the mutant mice became symptomatic; Fig. 1C). These results suggested that the abnormal neurons in these young *mafG*$^{-/-}$::*mafK*$^{+/-}$ mutant mice could be degenerating.

One of the most prominent histological features of many neurodegenerative disorders is the intracellular deposition of aggregated, ubiquitinated proteins (1). Since many neurons with swollen nuclei were observed in the symptomatic mice, we suspected that protein aggregates might have accumulated in their nuclei, and therefore we assessed these cells for evidence of ubiquitinated proteins. Indeed, spinal cord neurons of asymptomatic 3-week old *mafG*$^{-/-}$::*mafK*$^{+/-}$ mutant mice showed greatly elevated spinal cord ubiquitin immunostaining compared to those of their control littermates (Fig. 3F and E, respectively), primarily in the nuclei of the affected neurons (Fig. 3G). Ubiquitin immunostaining was also observed in the brain stem, thalamus, hippocampus, and subsections of the cerebral cortex of the mutants (data not shown).

Importantly, the distribution of the affected neurons in mutant mice that were identified by Nissl staining largely over-

lapped that of ubiquitin-positive cells. In contrast, no ubiquitin immunostaining was observed in Purkinje cells or granule cells of the cerebellum (data not shown). An increased high-molecular-weight smear of ubiquitin immunoreactivity was observed in whole-cell lysates prepared from *mafG*$^{-/-}$::*mafK*$^{+/-}$ mutant spinal cords in comparison to controls (data not shown). Thus the increased neuronal nuclear ubiquitin immunostaining in the mutant mice reflected coordinately increased accumulation of ubiquitinated protein aggregates in the same cells. Elevated ubiquitin levels were not detected in spinal cords of 1-week-old mutant mice, further supporting the hypothesis that pathological changes in these neurons are initially detectable around 3 weeks of age, coincident with the earliest onset of any nervous system phenotype (Fig. 1C).

A comparison between the expression profiles of MafK (22) and MafG (Fig. 2) taken together with the results of ubiquitin immunostaining suggested that the neurodegeneration was a cell-autonomous phenomenon. To substantiate this possibility, we performed double staining for both ubiquitin (using immunohistochemistry) and β-galactosidase (monitoring LacZ activity from the *mafG* knock-in) on sections from the spinal cords of 4-week-old *mafG*$^{-/-}$::*mafK*$^{+/-}$ mice. As shown Fig. 3H, almost all of the ubiquitin-positive cells also stained for LacZ activity. Taken together, these results strongly suggest that the neurodegeneration observed in the *mafG*$^{-/-}$::*mafK*$^{+/-}$ mice is cell autonomous.

Accumulation of ubiquitin conjugates suggested that the molecular mechanisms responsible for the neuronal degeneration observed in the *mafG*$^{-/-}$::*mafK*$^{+/-}$ mutant mice might have a common link to other neurodegenerative disorders. Therefore we assessed these same tissue sections for the presence of apoptotic neurons, whose presence is a common consequence of neurodegenerative diseases (21). We observed that neurons in the CA3 region of the hippocampus as well as several thalamic neurons were lost due to apoptosis by 6 weeks of age. Importantly however, we failed to detect a diminished number of neurons in the rest of the CNS, such as in the brain stem or spinal cord (data not shown). Consistent with these observations, neuronal loss was no more apparent in 30-week-old mutants than in the 10-week-old mutants. Thus the progressive and dosage-dependent defect in the small *maf* gene mutant mice differs from most neurodegenerative disorders in that, although the neurons display many cytopathological hallmarks of functional impairment, these are not accompanied by neuronal cell death.

Diminished expression of glycine receptor α 1 receptor in small *maf* gene mutant mice. We next addressed how the neurocytological abnormalities detected in the *mafG*$^{-/-}$::*mafK*$^{+/-}$ mutants might lead to the abnormal startle response since this was the single most prominent phenotype of these mutant mice. In surveying the literature describing phenotypes similar to those described here, we found several reports describing natural mouse mutants that display an abnormal response to startle stimuli, including mutations in the α (18, 30) and β subunit (17) genes of the murine inhibitory glycine receptors. Each of these *Glr* mutants displays long-lasting myoclonus and exaggerated startle responses. Glycine is a major inhibitory neurotransmitter in the spinal cord and brain stem, where its receptor is most abundant. Since neuronal degeneration was most prominent in the spinal cords and brain stems of these *mafG*$^{-/-}$::*mafK*$^{+/-}$ mutant mice, we conjectured that defective glycine receptor expression might account for at least a subset of the behavioral abnormalities displayed by the *maf* mutant animals.

To test the hypothesis that a small Maf deficiency might lead to diminished expression of inhibitory glycine receptors, we examined the steady *maf* accumulation of glycine receptor subunits in the small-*maf* gene mutant animals by RNA blot analysis. Diminished abundance of the Glra1 transcript in the brain stems of symptomatic mutant mice (Fig. 4A) was confirmed by quantitative analysis (Fig. 4B), although changes in Glrb transcript accumulation in symptomatic mutant mice was not statistically significant. The difference in abundance of mRNA expressed by one of the glutamate receptor genes (*NMDAR1*) between *mafG*$^{+/-}$::*mafK*$^{+/-}$ and *mafG*$^{-/-}$::*mafK*$^{+/-}$ mice was insignificant (Fig. 4A and B), suggesting that *Glra1* transcription was selectively diminished. Thus the reduction in Glra1 mRNA abundance (Fig. 4A) was directly reflective of reduced neuronal receptor abundance (Fig. 4C).

Finally, we examined Glra1 mRNA levels during the course of neonatal development. Since *Glra1* begins to be expressed between 2 and 3 weeks after birth, no expression was observed in newborns (Fig. 4D, lanes 1 to 4). At 3 weeks, *Glra1* expression in the mutant animals was slightly diminished in comparison to controls (Fig. 4D, lanes 5 to 8). However, by 10 weeks of age, Glra1 mRNA accumulation was significantly lower in the mutant CNS (Fig. 4D, lanes 11 and 12) than in the control (Fig. 4D, lanes 9 and 10) CNS. Therefore, *Glra1* reduction coincides with the progress of neuronal degeneration and phenotypic onset.

Small Maf loss in the CNS of affected mice results in selective alteration of MARE-dependent gene expression. Since MafG and MafK exert their function through homo- or heterodimeric binding to MAREs, we suspected that altering the molecular ratios between various large-subunit (CNC and Bach) transcription factors that interact with small Maf proteins might be distorted in *mafG*$^{-/-}$::*mafK*$^{+/-}$ mutant neurons (3, 24, 25). However, since it is not known whether or not *Glra1* is regulated by MARE(s), we examined the influence of altered small Maf abundance on MARE-dependent antioxidant gene regulation in the CNS. We showed previously that a large group of antioxidant-responsive genes are regulated through MAREs (10, 12), and, since an impaired defense mechanism against oxidative stress is regarded as a possible cause of neurodegeneration (1), we examined the expression of four well-characterized MARE-dependent oxidative stress-responsive genes in the *maf* mutants: genes encoding NAD(P)H quinone oxidoreductase (NQO1), MSP23 (also called peroxiredoxin I), glutathione *S*-transferase subunit Pi (GST-Pi), and heme oxygenase 1 (HO-1) (10). We found that *HO-1* gene expression was dramatically induced in 10-week-old *mafG*$^{-/-}$::*mafK*$^{+/-}$ mutant brains in comparison to *mafG*$^{+/-}$::*mafK*$^{+/-}$ control brains: *HO-1* induction was observed in the cerebrum, cerebellum, brain stem, and spinal cord (Fig. 5A, top). In surprising contrast, very little change in *GST-Pi* (Fig. 5A, middle) or *NQO1* or *MSP23* (data not shown) was detected.

To identify the cells expressing the most abundant HO-1 mRNA, we performed in situ hybridization analysis on brain stem sections. Strong staining was observed in neurons of *mafG*$^{-/-}$::*mafK*$^{+/-}$ mutant brains (Fig. 5B), but no staining

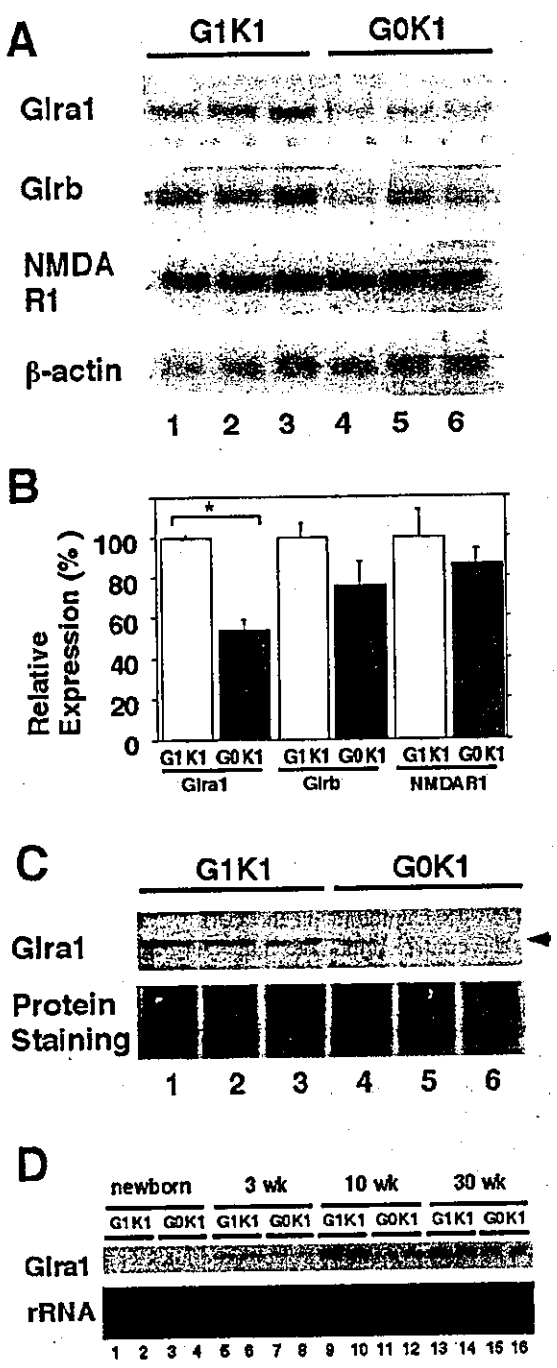

FIG. 4. Expression of glycine receptor α1 and β subunits in the CNS of small *maf* gene compound mutant mice. (A) RNA samples prepared from individual $mafG^{+/-}$::$mafK^{+/-}$ control mice (lanes 1 to 3) or $mafG^{-/-}$::$mafK^{+/-}$ mutant mice (lanes 4 to 6) were hybridized to probes corresponding to the *Glra1*, *Glrb*, or *NMDAR1* genes; these were normalized to β-actin expression as the internal control. (B) The data shown in panel A were quantified on a phosphorimager and then normalized to the internal control. *, $P < 0.05$. (C) The abundance of a Glra1 receptor subunit was examined by immunoblotting using an anti-α1 subunit antibody. Protein samples were prepared from individual $mafG^{+/-}$::$mafK^{+/-}$ control mice (lanes 1 to 3) and $mafG^{-/-}$::$mafK^{+/-}$ mutant mice (lanes 4 to 6). Protein staining was used to confirm equivalent protein loading. G0K1 and G1K1 are as defined for Fig. 1. (D) *Glra1* reduction was examined by RNA blot analysis using RNA samples prepared from the CNS of individual newborn mice (lanes 1 to 4) or animals 3 (lanes 5 to 8), 10 (lanes 9 to 12), or 30 weeks of age (lanes 13 to 16). RNA samples from $mafG^{+/-}$::$mafK^{+/-}$ control (lanes 1, 2, 5, 6, 9, 10, 13, and 14) and $mafG^{-/-}$::$mafK^{+/-}$ mutant littermates (lanes 3, 4, 7, 8, 11, 12, 15, and 16) were examined.

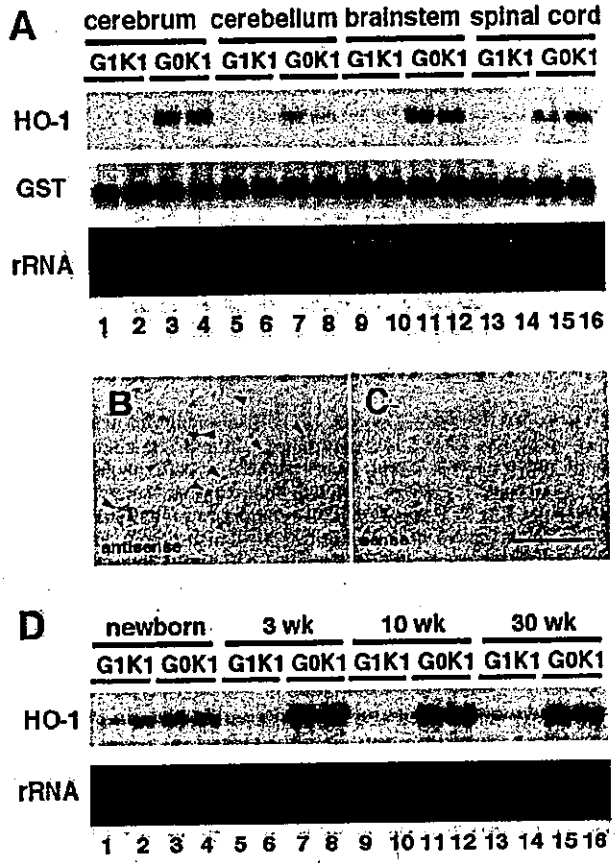

FIG. 5. HO-1 is induced in the $mafG^{-/-}$::$mafK^{+/-}$ mutant CNS. (A) RNA blot analysis was performed to examine the expression of *HO-1* and *GST-Pi* by using RNA samples prepared from the cerebrums (lanes 1 to 4), cerebellums (lanes 5 to 8), brain stems (lanes 9 to 12), and spinal cords (lanes 13 to 16) of individual 10-week-old $mafG^{+/-}$::$mafK^{+/-}$ control mice (lanes 1, 2, 5, 6, 9, 10, 13, and 14) and $mafG^{-/-}$::$mafK^{+/-}$ mutant mice (lanes 3, 4, 7, 8, 11, 12, 15, and 16). G0K1 and G1K1 are as defined for Fig. 1. (B and C) In situ hybridization was performed to examine the distribution of *HO-1*-expressing cells in the $mafG^{-/-}$::$mafK^{+/-}$ mutant brain stems at 5 weeks of age. Arrowheads, positively stained neurons. Scale bar (C), 60 μm. (D) *HO-1* induction was examined by RNA blot analysis using RNA samples prepared from the CNS of individual newborn mice (lanes 1 to 4) and animals 3 (lanes 5 to 8), 10 (lanes 9 to 12), or 30 weeks of age (lanes 13 to 16). RNA samples from $mafG^{+/-}$::$mafK^{+/-}$ controls (lanes 1, 2, 5, 6, 9, 10, 13, and 14) and $mafG^{-/-}$::$mafK^{+/-}$ mutant littermates (lanes 3, 4, 7, 8, 11, 12, 15, and 16) were examined.

above background was observed in neurons of the $mafG^{+/-}$::$mafK^{+/-}$ controls (data not shown). Hence, selective *HO-1* induction is observed only in CNS neurons of the affected $mafG^{-/-}$::$mafK^{+/-}$ mutant animals.

We then examined HO-1 mRNA levels during the course of neonatal development. In newborns, where no morphological

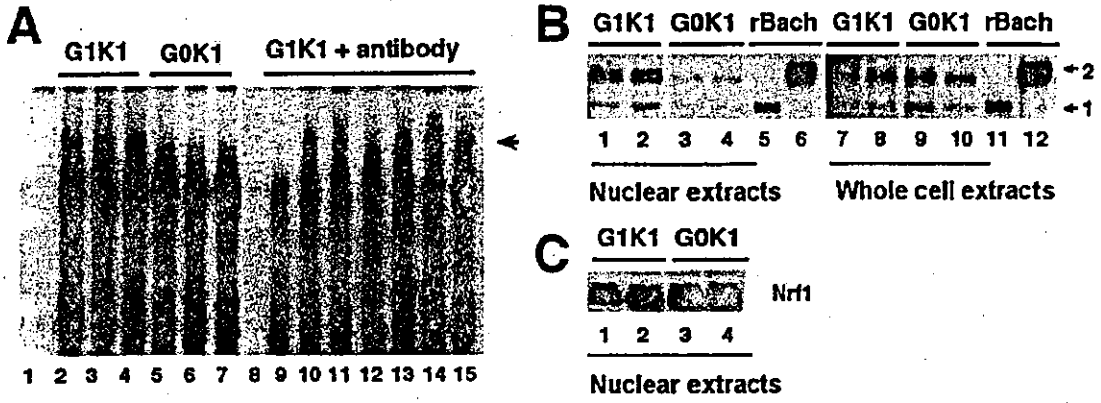

FIG. 6. MARE-binding activity of the Bach/small Maf heterodimer is reduced due to inhibition of Bach nuclear localization in the *maf* mutant mouse brain. (A) EMSA was performed with a probe containing a consensus MARE (see Materials and Methods). The probe was incubated without added nuclear extract (lanes 1 and 8) or with nuclear extract prepared from *mafG*$^{+/-}$::*mafK*$^{+/-}$ control mouse brains (lanes 2 to 4 and 9 to 15) and *mafG*$^{-/-}$::*mafK*$^{+/-}$ mutant mouse brains (lanes 5 to 7). The intensity of the lowest-mobility complex (arrow) was reduced in the mutant brains (lanes 5 to 7). Formation of this complex was inhibited by preincubation of extracts with an anti-small Maf antibody (lane 9) or an anti-Bach antibody (lane 12) but not with anti-p45 NF-E2, anti-Nrf1, anti-Fos, anti-Jun, or preimmune antibodies (lanes 10, 11, 13, 14, and 15, respectively). G0K1 and G1K1 are as defined for Fig. 1. (B and C) Nuclear extracts (lanes 1 to 4) and whole-cell extracts (lanes 7 to 10) were prepared from control *mafG*$^{+/-}$::*mafK*$^{+/-}$ mouse brains (lanes 1, 2, 7, and 8) or *mafG*$^{-/-}$::*mafK*$^{+/-}$ mutant mouse brains (lanes 3, 4, 9, and 10). Recombinant Bach1 and Bach2 proteins served as the positive control (rBach; lanes 5, 6, 11, and 12). Anti-Bach (B) and anti-Nrf1 (C) antibodies were used for immunoblot analysis. Arrows 1 and 2, mobilities of Bach1 and Bach2, respectively.

or phenotypic changes are yet apparent in the *maf* mutant brain, *HO-1* expression was slightly elevated in comparison to controls (Fig. 5D, lanes 1 to 4). However, after 3 weeks of age, the earliest detectable time of any neuropathology in these mice, HO-1 mRNA accumulation was significantly higher in the mutant (Fig. 5D, lanes 7 and 8) than in the control CNS (Fig. 5D, lanes 5 and 6), and this differential expression persisted into adulthood (Fig. 5D, lanes 9 to 16). Therefore, *HO-1* induction preceded the onset of any morphological changes in affected CNS neurons and became prominent coincident with the time of progressing neuronal degeneration and phenotypic onset. These results strongly suggested that the disturbance of MARE-dependent transcriptional regulation was responsible for the failure to maintain normal CNS function in the *maf* mutant mice.

Bach/small Maf heterodimers are reduced in abundance in the *maf* mutant CNS. We next examined MARE-dependent binding activities in *mafG*$^{-/-}$::*mafK*$^{+/-}$ brain extracts. We performed EMSA using a consensus MARE sequence as the probe (see Materials and Methods). Using nuclear extracts prepared from compound heterozygous mutant (control) brains, we found that several proteins formed complexes with the MARE (Fig. 6A, lanes 2 to 4). When equivalent samples from the *mafG*$^{-/-}$::*mafK*$^{+/-}$ mutant mice were examined in kind, only the lowest-mobility band was significantly altered in intensity (Fig. 6A, lanes 5 to 7). This complex was specifically inhibited by the addition of an excess of an unlabeled MARE-containing oligonucleotide but not by a scrambled oligonucleotide (data not shown), indicating that this binding activity was specific for the MARE sequence.

When an antibody against the small Maf proteins was included in the EMSA reaction, most of the complexes (including the entire lowest-mobility band) diminished in intensity (Fig. 6A, lane 9), demonstrating that small Mafs participate in these complexes. Addition of an antibody that recognizes both Bach proteins (29) interfered with formation of the lowest-mobility complex (Fig. 6A, lane 12). In contrast, this same complex was unaltered when antibodies recognizing p45 NF-E2, Nrf1, c-Jun, or c-Fos were preincubated with the extracts (Fig. 6A, lanes 10, 11, 13, and 14, respectively). These data indicated that the electrophoretically distinct lowest-mobility complex contained both small Maf and Bach proteins and was significantly less abundant in the *mafG*$^{-/-}$::*mafK*$^{+/-}$ mutant than in the control brain. We tentatively concluded that the reduction in abundance of Bach/small Maf heterodimers in the mutants might represent a key biochemical deficiency, thus altering the normal transcription of genes regulated by MAREs in the CNS of the *mafG*$^{-/-}$::*mafK*$^{+/-}$ mutant mice.

Suppression of Bach protein nuclear localization in small *maf* gene mutant brains. To test the hypothesis that diminished Bach/small Maf complex formation might be attributable to reduced small Maf abundance in the mutant CNS, we next asked whether or not the abundance of Bach proteins in the mutants was altered (since Bach homodimers cannot bind to MAREs [29]). To this end, we compared nuclear extracts prepared from the brains of mutant and control mice by immunoblotting using an anti-Bach antibody. The levels of both Bach1 and Bach2 were significantly reduced in *mafG*$^{-/-}$::*mafK*$^{+/-}$ mutant brain nuclear extracts compared to those in *mafG*$^{+/-}$::*mafK*$^{+/-}$ controls (Fig. 6B, lanes 1 to 6), while the abundance of another CNC family protein, Nrf1, in mice with the two genotypes was unchanged (Fig. 6C). When we repeated the immunoblot analysis with whole-cell extracts instead of nuclear extracts, we were surprised to find that there was no difference in Bach protein abundance between the two samples (Fig. 6B, lanes 7 to 12). We tentatively concluded that the Bach proteins, normally found exclusively in the nucleus, reside predominantly in the cytoplasm in the neurons of *mafG*$^{-/-}$::*mafK*$^{+/-}$ mutant mice. If true, this conclusion also implied that stable nuclear accumulation of the Bach proteins

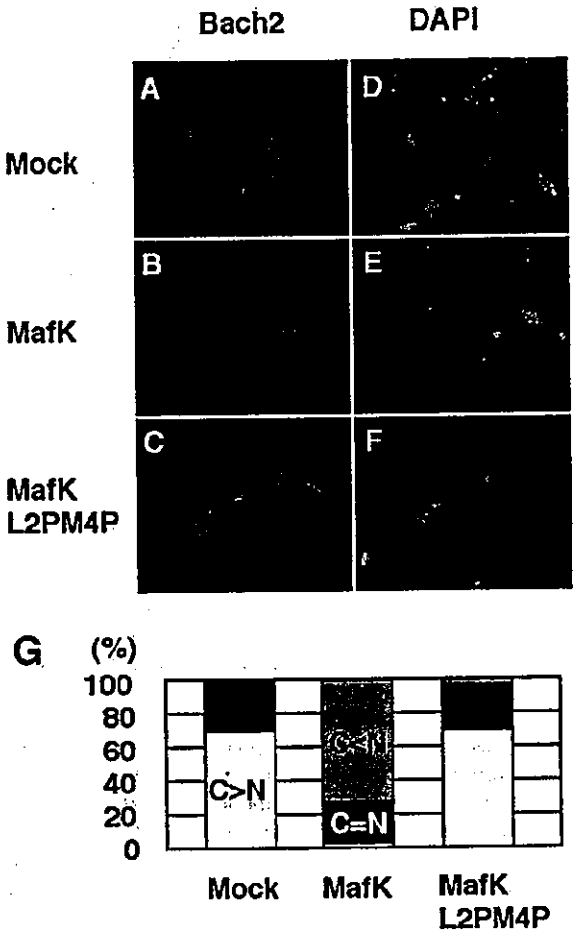

FIG. 7. Small Maf proteins promote nuclear localization of Bach2. NIH 3T3 cells were examined for subcellular localization of transfected Bach2 protein (A to C) or location of nuclei in these cells using DAPI (D to F). The Bach2 expression plasmid was either transfected alone (A and D) or cotransfected with a vector directing expression of *mafK* (B and E) or a *mafK* mutant in two positions that disrupts dimerization (MafKL2PM4P; C and F). (G) Quantitative analysis of subcellular localization of Bach2. A total of 100 transfected cells were examined for Bach2 localization and classified into three different categories: C>N, predominantly cytoplasmic; C=N, equally distributed; C<N, predominantly nuclear.

depends directly on the availability and/or abundance of small Maf proteins.

Small Maf proteins promote nuclear localization of Bach proteins. To test the hypothesis that small Maf proteins can affect the subcellular distribution of Bach factors, Bach2 was transiently expressed in NIH 3T3 cells and its subcellular localization was determined by indirect immunofluorescence using the anti-Bach antibody. When Bach2 alone was transfected, immunostaining was observed exclusively in the cytoplasm as previously reported (Fig. 7A and D) (7). In contrast, when Bach2 was transfected with MafK, Bach2 accumulated predominantly within nuclei (Fig. 7B and E). The same result was observed when Bach2 and MafG were coexpressed (not shown), while coexpression of Bach2 with the MafK leucine zipper mutant, MafKL2PM4P (23), which fails to heterodimerize with Bach or CNC proteins, failed to promote Bach2 nuclear localization (Fig. 7C and F). When Bach1 was transfected instead of Bach2, MafG and MafK had effects identical to those that they had on Bach2 cellular localization (data not shown). Taken together, these results demonstrate that the small Maf proteins promote translocalization of Bach1 and Bach2 from the cytoplasm into the nucleus and that the leucine zipper motif of the small Mafs is essential for this function. These results suggested an intriguing possibility for a novel function of the small Maf proteins in transcriptional regulation: besides being required for binding site specificity for the MARE (extended AP-1) sequence (25), they may promote preferred nuclear localization of heterodimeric partner subunits (CNC and Bach family members) that are required for transcriptional activation and repression.

DISCUSSION

In this study, we focused on a progressive neurological disorder that we first detected in *mafG* homozygous mutant mice (31) and that was quite dramatically exacerbated in *mafG*::*mafK* compound mutant animals (28). While the neurological symptoms in *mafG*$^{-/-}$ mice were detectable in only a fraction of the mutant animals and only after they reached 25 weeks or more of age, a more extreme version of essentially the same neuropathology was fully developed by 9 weeks of age in *mafG*$^{-/-}$::*mafK*$^{+/-}$ mice with >90% penetrance. One characteristic of this neuropathology was intermittent and long-lasting myoclonus, which could be triggered by external or internal stimuli. This phenotype immediately suggested that neuronal excitability was abnormally facilitated or that inhibitory inputs to neuromotor function were defective.

Since we found that the *maf* mutants displayed abnormal startle responses that could be triggered by acoustic stimuli, we searched for natural mutants that were reported to have similar characteristics. The example of natural mutant mice with defective glycine receptor subunit genes (*Glra1 and Glrb*) was most intriguing (17, 18, 30). Glycine is a major inhibitory neurotransmitter after birth, affecting transmission in the spinal cord and brain stem. The glycine postsynaptic receptor consists of ligand-binding α and structural β subunits, which assemble to form a glycine-gated chloride channel. Mice homozygous for *oscillator* (*spd*^{ot}), a null mutation in the *Glra1* gene, develop severe tremors and die by 3 weeks of age, while heterozygous *oscillator* animals display no abnormal behavior but have an increased acoustic startle response, conferred by a haploinsufficiency in glycine receptor function (18). We therefore suspected that aspects of the phenotype observed in *mafG*$^{-/-}$::*mafK*$^{+/-}$ mice might be caused by diminished glycine receptor expression.

As anticipated, we found reduced glycine receptor expression in the CNS of *mafG*$^{-/-}$::*mafK*$^{+/-}$ mice. The phenotype observed in these mutant mice was more severe than that observed in heterozygous *spd*^{ot} mice but milder than that observed in the homozygous mutant animals. This intermediate phenotype may indicate that α 1 receptor expression in *mafG*$^{-/-}$::*mafK*$^{+/-}$ mice is severely reduced but not completely eliminated. Diminished β subunit expression may also contribute to the symptoms of *mafG*$^{-/-}$::*mafK*$^{+/-}$ mice, although we were unable to document a statistically significant

difference in *Glrb* abundance. In this regard, it has been shown that *Glrb* transgene-complemented *spastic* mice that retain 25% of wild-type Glr activity display little phenotype (2), suggesting that the twofold Glr reduction exhibited in the *mafG*$^{-/-}$::*mafK*$^{+/-}$ mutants must be at most only partially responsible for the complex neuromotor disturbance reported here.

Reduced glycine receptor accumulation in the *maf* mutants could be a direct consequence of small Maf deficiency or a reflection of protein aggregation in neuronal nuclei that indirectly interferes with cellular processes that ultimately impair the functionality of these proteins. Since very little is known about the transcriptional regulatory mechanisms controlling *Glra1* and *Glrb*, we cannot distinguish between these possibilities at present (attempts to identify MAREs in the two promoters by simple sequence searches failed to reveal genuine small Maf regulatory target sites). It should be noted that neurological signs observed in *mafG*$^{-/-}$::*mafK*$^{+/-}$ mice did not completely overlap with those in the natural glycine receptor mutants. In particular, affected neurons are distributed throughout the CNS, not only in the spinal cords and brain stems, of *mafG*$^{-/-}$::*mafK*$^{+/-}$ mice. However, we found that the CA3 region of the hippocampus and a part of the thalamus both suffer almost complete cellular loss from apoptosis in the mutant, but not in the control, animals (data not shown). Thus lesions in other regions of the brain may be responsible for additional neurological abnormalities that lead to complex phenotypes in these mice that we have not yet deciphered. To better understand the molecular origins of the compound *maf* mutant phenotypes, we are in the process of detailed comparisons to several mouse neurological mutations (*oscillator*, *stargazer*, *spasmodic*, and *spastic*) (2, 17, 18, 30) whose phenotypes each display overlapping similarities to the phenotypes reported here.

Histological examination of the small *maf* gene compound mutants revealed that neurons in the spinal cord, brain stem, and other parts of the CNS became chromatolytic and that ubiquitinated protein aggregates increased in the nuclei of these affected neurons. Accumulation of aggregated proteins is frequently observed in neurodegenerative diseases (1), and three major factors have been proposed for the formation of inclusion bodies or extracellular aggregates: one is that a mutated gene product itself aggregates, a second is that proteins become oxidized and denatured due to oxidative stress, and a third is that protein degradation mechanisms are somehow rendered defective. In the *mafG*$^{-/-}$::*mafK*$^{+/-}$ mutant mice, we anticipated that general neuronal defense mechanisms against oxidative stress might be impaired since most antioxidant-responsive genes are regulated through MARE sequences (11, 24). To our surprise, however, we detected changes in the expression of only one of the four antioxidant genes examined, *HO-1* (see below). We concluded from these data that cytological changes in neurons of the *mafG*$^{-/-}$::*mafK*$^{+/-}$ mutant mice share some, but not all, of the characteristics that are often found in human neurodegenerative disorders. Although we first anticipated that reduced expression of MARE-dependent genes in neurons might lead to neuronal degeneration, all of the MARE-dependent target genes we examined were unchanged except for *HO-1*, and there was no apparent age-dependent reduction in the number of neurons through either cell death or apoptosis. Unexpectedly, *HO-1* was markedly induced, coincident with a clear reduction in the Bach/small Maf EMSA complex, in brain nuclear extracts prepared from the *mafG*$^{-/-}$::*mafK*$^{+/-}$ mutant mice. Since Bach proteins are expressed in neurons (29), as are MafK and MafG (25) (Fig. 2), Bach/small Maf heterodimers were predicted to exist in neuronal cells. Bach family proteins are reported to be transcriptional repressors (29), and thus any reduction in the amount of Bach/small Maf heterodimers would be expected to lead to relief of repression (induction) of Bach/small Maf-regulated MARE-dependent genes. Recently, we reported that Bach1 null mutant mice also exhibit increased HO-1 mRNA accumulation (34). In that report, we performed chromatin immunoprecipitation assays to demonstrate that small Maf proteins bind to the functional MARE sequence located in the *HO-1* regulatory sequences (34). *HO-1* induction in the *maf* mutant mice serves as clear complementary evidence for disturbance of this MARE-dependent regulatory event. While increased *HO-1* gene expression might contribute to increased cytotoxicity (35), abundant HO-1 itself may not be an underlying cause for the observed neuronal deterioration in the *maf* mutants, since HO-1 also plays a role in cytoprotection against oxidative stress (35). Dysregulation of some currently unidentified MARE-dependent gene(s) (encoding glycine receptor subunits, proteasome components, or other factors in this circuitry) may be the primary pathogenic event.

Although diminished expression of Bach/small Maf heterodimers was the most readily apparent alteration in the EMSA pattern of *maf* mutant brain extracts, we cannot overlook the far more abundant contribution of CNC regulatory proteins that partner with small Mafs (Nrf1, Nrf2, and Nrf3) to regulate transcription through MAREs (e.g., the most abundant gel shift product in Fig. 6A), since all of these CNC family members are also expressed in the brain. The antiserum against the small Maf proteins reacts not only with the low-mobility Bach/small Maf heterodimer but also with all the other more abundant complexes (Fig. 6A, lane 9). Since the intensity of this broad, higher-mobility band in the *mafG*$^{-/-}$::*mafK*$^{+/-}$ brain extracts was essentially the same as that in control extracts, one initial assumption might be that the corresponding binding activities in the mutant extracts may be unchanged. However, since the tissue extracts are not purely neuronal, contributions from glia might mask even quite significant neuronal depletion of any of the CNC proteins. If this were the case, then altered neuronal composition of the higher-mobility band could also be a contributing factor to the observed neuronal deterioration. To address the question of which MARE-interacting proteins are directly responsible for the motor disorder, we would need to know the detailed consequences of mutations in each of these *CNC* genes in the CNS, but, to date, germ line mutation of the *CNC* genes has failed to display neurological phenotypes (5, 11, 32, 33).

We showed that small Maf proteins facilitated nuclear localization of Bach proteins in vivo and in vitro, revealing another novel aspect of small Maf function in transcriptional regulation. Bach1 and Bach2 both have nuclear and cytoplasmic localization signals (NLS and CLS, respectively) (7), and Bach2 nuclear localization is regulated by the cellular nuclear export system through its CLS in response to stimuli such as oxidative stress (7). It was also reported that Bach1t, which lacks a CLS, confers a preferred nuclear localization to Bach1,

and the hypothesis that subcellular localization of Bach is determined by the net balance between NLS and CLS activity was proposed (13). This hypothesis can now be extended if we incorporate the properties of the Bach/small Maf complex described here. We showed that, under normal conditions, the Bach proteins, possessing one CLS and one NLS, are preferentially localized in the cytoplasmic compartment (presumably because of greater CLS activity or lesser NLS activity). After Bach proteins heterodimerize with small Mafs, which possess only an NLS, the two proteins together now bear two NLS and one CLS. We infer that the two-to-one ratio between NLS and CLS activities within this heterodimeric complex may be required for stable nuclear accumulation of Bach proteins. Since MafKL2PM4P, a leucine zipper MafK mutant, was unable to facilitate nuclear import of Bach, we conclude that heterodimerization between Bach and small Maf proteins is essential for the nuclear confinement of Bach proteins, supporting this NLS-CLS "balance" hypothesis.

This study provides the first insights detailing the significance of MARE-dependent transcriptional regulation in the execution of normal CNS function. In this work, we chose to examine *mafG*$^{-/-}$::*mafK*$^{+/-}$ mice for the analysis of a specific neurological disorder. Although this severe motor phenotype is fully penetrant in *mafG*$^{-/-}$::*mafK*$^{+/-}$ mice, the mice still have an almost-normal life span. When an even greater number of defective small *maf* alleles are introduced into this background, the effect is lethal, either before weaning or in utero (28; F. Katsuoka and H. Motohashi, unpublished data). The degree of small Maf reduction in the *mafG*$^{-/-}$::*mafK*$^{+/-}$ mutant mice was optimal for generating the neuropathology we wished to analyze. Thus one important conclusion of this work is that hypomorphic mutants, created by combining lesions in multiple genes that are likely to be compensatory may serve as a powerful tool for analyzing the pathogenesis of adult human diseases, since these experimental animals exhibit specifically impaired cellular functions and yet survive.

ACKNOWLEDGMENTS

We are grateful to Kim-Chew Lim and M. Masu for critical discussions and advice. We thank T. Ishii for providing the HO-1 cDNA and S. Nakanishi for providing the NMDAR1 cDNA. We also thank N. Kaneko for technical support in histological analysis and R. Kawai for mouse breeding.

This work was supported by NIH grant CA80088 to J.D.E., grants from the Ministry of Education, Culture, Sports, Science and Technology (H.M. and M.Y.), JSPS-RFTF, and CREST (M.Y.), and the Special Coordination Fund for Promoting Science and Technology and PROBRAIN (H.M.).

REFERENCES

1. **Alves-Rodrigues, A., L. Gregori, and M. E. Figueiredo-Pereira.** 1998. Ubiquitin, cellular inclusions and their role in neurodegeneration. Trends Neurosci. 21:516–520.
2. **Becker, L., B. Hartenstein, J. Schenkel, J. Kuhse, H. Betz, and H. Weiher.** 2000. Transient neuromotor phenotype in transgenic spastic mice expressing low levels of glycine receptor beta-subunit: an animal model of startle disease. Eur. J. Neurosci. 12:27–32.
3. **Blank, V., and N. C. Andrews.** 1997. The Maf transcription factors: regulators of differentiation. Trends Biochem. Sci. 22:437–441.
4. **Dignam, J. D.** 1990. Preparation of extracts from higher eukaryotes. Methods Enzymol. 182:194–203.
5. **Farmer, S. C., C.-W. Sun, G. E. Winnier, B. L. M. Hogan, and T. M. Townes.** 1997. The bZip transcription factor LCR-F1 is essential for mesoderm formation in mouse development. Genes Dev. 11:786–798.
6. **Fukumauchi, F., N. Mataga, Y. J. Wang, S. Sato, A. Youshiki, and M. Kusakabe.** 1996. Abnormal behavior and neurotransmissions of tenascin gene knockout mouse. Biochem. Biophys. Res. Commun. 221:151–156.
7. **Hoshino, H., A. Kobayashi, M. Yoshida, N. Kudo, T. Oyake, H. Motohashi, N. Hayashi, M. Yamamoto, and K. Igarashi.** 2000. Oxidative stress abolishes leptomycin B-sensitive nuclear export of transcription repressor Bach2 that counteracts activation of Maf recognition element. J. Biol. Chem. 275: 15370–15376.
8. **Igarashi, K., K. Itoh, N. Hayashi, M. Nishizawa, and M. Yamamoto.** 1995. Conditional expression of the ubiquitous transcription factor MafK induces erythroleukemia cell differentiation. Proc. Natl. Acad. Sci. USA 92:7445–7449.
9. **Igarashi, K., K. Itoh, H. Motohashi, N. Hayashi, Y. Matuzaki, H. Nakauchi, M. Nishizawa, and M. Yamamoto.** 1995. Activity and expression of murine small Maf family protein MafK. J. Biol. Chem. 270:7615–7624.
10. **Ishii, T., K. Itoh, S. Takahashi, H. Sato, T. Yanagawa, Y. Katoh, S. Bannai, and M. Yamamoto.** 2000. Transcription factor Nrf2 coordinately regulates a group of oxidative stress-inducible genes in macrophages. J. Biol. Chem. 275:16023–16029.
11. **Itoh, K., T. Chiba, S. Takahashi, T. Ishii, K. Igarashi, Y. Katoh, T. Oyake, N. Hayashi, K. Satoh, I. Hatayama, M. Yamamoto, and Y. Nabeshima.** 1997. An Nrf2/small Maf heterodimer mediates the induction of phase II detoxifying enzyme genes through antioxidant response elements. Biochem. Biophys. Res. Commun. 236:313–322.
12. **Itoh, K., T. Ishii, N. Wakabayashi, and M. Yamamoto.** 1999. Regulatory mechanisms of cellular response to oxidative stress. Free Radic. Res. 31: 319–324.
13. **Kanezaki, R., T. Toki, M. Yokoyama, K. Yomogida, K. Sugiyama, M. Yamamoto, K. Igarashi, and E. Ito.** 2001. Transcription factor BACH1 is recruited to the nucleus by its novel alternative spliced isoform. J. Biol. Chem. 276:7278–7284.
14. **Kataoka, K., K. Igarashi, K. Itoh, K. T. Fujiwara, M. Noda, M. Yamamoto, and M. Nishizawa.** 1995. Small Maf proteins heterodimerize with Fos and may act as competitive repressors of the NF-E2 transcription factor. Mol. Cell. Biol. 15:2180–2190.
15. **Katsuoka, F., H. Motohashi, K. Onodera, N. Suwabe, J. D. Engel, and M. Yamamoto.** 2000. One enhancer mediates *mafK* transcriptional activation in both hematopoietic and cardiac muscle cells. EMBO J. 19:2980–2991.
16. **Kawai, S., N. Goto, K. Kataoka, T. Sacgusa, H. Shinno-Kohno, and M. Nishizawa.** 1992. Isolation of the avian transforming retrovirus, AS42, carrying the *v-maf* oncogene and initial characterization of its gene product. Virology 188:778–784.
17. **Kingsmore, S. F., B. Giros, D. Suh, M. Bieniarz, M. G. Caron, and M. F. Seldin.** 1994. Glycine receptor β-subunit gene mutation in spastic mouse associated with LINE-1 element insertion. Nat. Genet. 7:136–141.
18. **Kling, C., M. Koch, B. Saul, and C. M. Becker.** 1997. The frameshift mutation oscillator *Glra1*$^{spd\text{-}ot}$ produces a complete loss of glycine receptor α 1-polypeptide in mouse central nervous system. Neuroscience 78:411–417.
19. **Kotkow, K. J., and S. H. Orkin.** 1996. Complexity of the erythroid transcription factor NF-E2 as revealed by gene targeting of the mouse p18 NF-E2 locus. Proc. Natl. Acad. Sci. USA 93:3514–3518.
20. **Masuo, Y., Y. Matsumoto, S. Morita, and J. Noguchi.** 1997. A novel method for counting spontaneous motor activity in the rat. Brain Res. Brain Res. Protoc. 1:321–326.
21. **Mattson, M. P.** 2000. Apoptosis in neurodegenerative disorders. Nat. Rev. Mol. Cell Biol. 1:120–129.
22. **Motohashi, H., K. Igarashi, K. Onodera, S. Takahashi, H. Ohtani, M. Nakafuku, M. Nishizawa, J. D. Engel, and M. Yamamoto.** 1996. Mesodermal- vs neuronal-specific expression of MafK is elicited by different promoters. Genes Cells 1:223–238.
23. **Motohashi, H., F. Katsuoka, J. A. Shavit, J. D. Engel, and M. Yamamoto.** 2000. Positive or negative MARE-dependent transcriptional regulation is determined by the abundance of small Maf proteins. Cell 103:865–875.
24. **Motohashi, H., T. O'Connor, F. Katsuoka, J. D. Engel, and M. Yamamoto.** 2002. Integration and diversity of the regulatory network composed of Maf and CNC families of transcription factors. Gene 294:1–12.
25. **Motohashi, H., J. A. Shavit, K. Igarashi, M. Yamamoto, and J. D. Engel.** 1997. The world according to Maf. Nucleic Acids Res. 25:2953–2959.
26. **Noebels, J. L., X. Qiao, R. T. Bronson, C. Spencer, and M. T. Davisson.** 1990. Stargazer: a new neurological mutant on chromosome 15 in the mouse with prolonged cortical seizures. Epilepsy Res. 7:129–135.
27. **Onodera, K., J. A. Shavit, H. Motohashi, F. Katsuoka, J. E. Akasaka, J. D. Engel, and M. Yamamoto.** 1999. Characterization of the murine *mafF* gene. J. Biol. Chem. 274:21162–21169.
28. **Onodera, K., J. A. Shavit, H. Motohashi, M. Yamamoto, and J. D. Engel.** 2000. Perinatal synthetic lethality and hematopoietic defects in compound *mafG::mafK* mutant mice. EMBO J. 19:1335–1345.
29. **Oyake, T., K. Itoh, H. Motohashi, N. Hayashi, H. Hoshino, M. Nishizawa, M. Yamamoto, and K. Igarashi.** 1996. Bach proteins belong to a novel family of BTB-basic leucine zipper transcription factors that interact with MafK and regulate transcription through the NF-E2 site. Mol. Cell. Biol. 16:6083–6095.
30. **Ryan, S. G., M. S. Buckwalter, J. W. Lynch, C. A. Handford, L. Segura, R.**

Shiang, J. J. Wasmuth, S. A. Camper, P. Schofield, and P. O'Connell. 1994. A missense mutation in the gene encoding the α 1 subunit of the inhibitory glycine receptor in the spasmodic mouse. Nat. Genet. 7:131–135.
31. Shavit, J. A., H. Motohashi, K. Onodera, J. Akasaka, M. Yamamoto, and J. D. Engel. 1998. Impaired megakaryopoiesis and behavioral defects in *mafG*-null mutant mice. Genes Dev. 12:2164–2174.
32. Shivdasani, R. A., and S. H. Orkin. 1995. Erythropoiesis and globin gene expression in mice lacking the transcription factor NF-E2. Proc. Natl. Acad. Sci. USA 92:8690–8694.
33. Shivdasani, R. A., M. F. Rosenblatt, D. Zucker-Franklin, C. W. Jackson, P. Hunt, C. J. Saris, and S. H. Orkin. 1995. Transcription factor NF-E2 is required for platelet formation independent of the actions of thrombopoietin/MGDF in megakaryocyte development. Cell 81:695–704.
34. Sun, J., H. Hoshino, K. Takaku, O. Nakajima, A. Muto, H. Suzuki, S. Tashiro, S. Takahashi, S. Shibahara, J. Alam, M. Taketo, M. Yamamoto, and K. Igarashi. 2002. Hemoprotein Bach1 regulates enhancer availability of heme oxygenase-1 gene. EMBO J. 21:5216–5224.
35. Suttner, D. M., and P. A. Dennery. 1999. Reversal of HO-1 related cytoprotection with increased expression is due to reactive iron. FASEB J. 13:1800–1809.

Carcinogenesis vol.24 no.3 pp.461–467, 2003

Interactive effects of *nrf2* genotype and oltipraz on benzo[*a*]pyrene–DNA adducts and tumor yield in mice

Minerva Ramos-Gomez[1]*, Patrick M.Dolan[1], Ken Itoh[2], Masayuki Yamamoto[2] and Thomas W.Kensler[1,3]

[1]Department of Environmental Health Sciences, Bloomberg School of Public Health, The Johns Hopkins University, Baltimore, MD 21202, USA and [2]Center for TARA, Tsukuba University, Tsukuba 305, Japan
*Current address: Division de Estudios de Posgrado, Facultad de Quimica, Universidad Anutonoma de Queretaro, Cerro de las Campanas s/n, Queretaro, Qro. C.P. 7608 Mexico

[3]To whom correspondence should be addressed
Email: tkensler@jhsph.edu

The cancer chemopreventive actions of oltipraz (4-methyl-5-[2-pyrazinyl]-1,2-dithiole-3-thione) have been primarily associated with the induction of phase 2 detoxifying enzymes through transcriptional activation of the antioxidant response element (ARE) in the promoter regions of these genes. The transcription factor Nrf2 has been shown to bind to and activate AREs. Previously, we demonstrated that *nrf2*-deficient mice had low basal expression of phase 2 enzymes and were substantially more susceptible to benzo[*a*]pyrene (B[*a*]P)-induced neoplasia of the forestomach than wild-type. Moreover, loss of Nrf2 abrogated the chemopreventive action of oltipraz, when administered 48 h before B[*a*]P, an interval allowing maximal induction of many phase 2 enzymes. Oltipraz also inhibits some cytochrome P450s involved in the bioactivation of B[*a*]P. In the present study we observed that oltipraz had no protective effect on tumor burden in the forestomach of *nrf2*-deficient mice when administered 1 h before B[*a*]P, a timeline that selectively optimizes for possible inhibitory effects on cytochrome P450s. To evaluate the role of *nrf2* genotype on B[*a*]P disposition, levels of B[*a*]P–DNA adducts were measured as tetrols released from DNA isolated from target (forestomach) and non-target tissues (liver) of wild-type and *nrf2*-deficient mice treated with either vehicle or oltipraz 1 or 48 h before B[*a*]P. Levels of B[*a*]P–DNA adducts in forestomach were significantly higher in *nrf2*-deficient compared with wild-type mice. Oltipraz treatment at 1 or 48 h before B[*a*]P had no protective effect on forestomach tetrol levels in *nrf2*-deficient mice, whereas a significant reduction was observed in wild-type mice treated with oltipraz 48 h, but not 1 h, before carcinogen. Combining all treatments and genotypes, there was a strong correlation (R^2 = 0.91) between levels of B[*a*]P–DNA adducts in forestomach and subsequent yield of tumors. In contrast to the results in forestomach, *nrf2* genotype did not modify hepatic B[*a*]P–DNA adduct levels while both oltipraz treatments were protective, suggesting that Nrf2-independent mechanisms (e.g. P450 inhibition) for oltipraz can also occur *in vivo* in some tissues.

Abbreviations: ARE, antioxidant response element; B[*a*]P, benzo[*a*]pyrene; (t)-trans-B[*a*]P-7,8-diol, (±)-*trans*-7,8-dihydroxy-7,8-dihydrobenzo[*a*]pyrene; CYP, cytochrome P450; GST, glutathione *S*-transferase; HPLC, high-pressure liquid chromatography; NQO1, NAD(P)H:quinone oxidoreductase; oltipraz, 4-methyl-5-[2-pyrazinyl]-1,2-dithiole-3-thione; TA, *trans-anti*-B[*a*]P-tetrol.

Introduction

Cancer chemoprevention is a strategy for cancer control that utilizes chemical agents to block, retard or even reverse the carcinogenic process through the administration of one or several compounds. Many classes of cancer chemopreventive agents including phenolic antioxidants, 1,2-dithiole-3-thiones, isothiocynates, flavones and coumarins are effective at blocking DNA damaging steps in the carcinogenic process by modulating the metabolic activation and detoxication of carcinogenic substances. Oltipraz (4-methyl-5-[2-pyrazinyl]-1,2-dithiole-3-thione), a substituted 1,2-dithiole-3-thione, is known to inhibit experimental tumorigenicity elicited by many structurally diverse carcinogens in numerous target tissues (1–3). The chemopreventive actions of oltipraz have been largely associated with the induction of phase 2 detoxifying enzymes, such as, glutathione *S*-transferase (GST), NAD(P)H:quinone oxidoreductase (NQO1) and UDP-glucuronosyltransferase (UGT), as well as epoxide hydrolase (4–6).

Increased expression of phase 2 detoxifying enzymes is primarily the result of transcriptional activation of their corresponding genes. This increased expression is mediated, in part, by an ARE (antioxidant response element) in their promoter regions (7–9) and the Nrf2 transcription factor has been shown to bind to and activate ARE sequences of these genes (10,11). Nrf2, a member of the basic-leucine zipper family of transcription factors, has been shown to heterodimerize with members of the small Maf family proteins (12–14). The involvement of Nrf2–Maf heterodimers in the ARE-mediated regulation of phase 2 detoxifying enzymes, as well as of oxidative stress responsive proteins, has been confirmed by studies using *nrf2* knockout mice. Significantly reduced expression and inducibility of NQO1, GST subunits and γ-glutamylcysteine synthetase in mice lacking Nrf2 indicates an *in vivo* role of this transcription factor in the regulation of these genes (11,15–19).

Studies in *nrf2*-disrupted mice have demonstrated the important role of Nrf2 in protection against different chemical toxicities, such as acute pulmonary injury by the food preservative butylated hydroxytoluene (20) or by hyperoxic conditions (21); to DNA adduct formation in lung after exposure to diesel exhaust (22); the vulnerability of *nrf2* knockout to acetaminophen hepatotoxicity (23,24); and in inflammation during the wound repair process in skin (25). In addition to these findings, we reported previously that *nrf2*-deficient mice were more susceptible to benzo[*a*]pyrene (B[*a*]P)-induced neoplasia of the forestomach than wild-type mice. This increased susceptibility was associated with low basal expression of several phase 2 gene transcripts as well as low total GST and NQO1 enzymatic activities in the stomach (26). Moreover, we observed that loss of expression of Nrf2 completely abrogated the chemopreventive actions of oltipraz when administered 48 h before B[*a*]P, an interval allowing maximal induction of many phase 2 enzymes. Using a similar experimental system, Fahey *et al.* (27) observed that sulforaphane,

an isothiocyanate isolated from cruciferous vegetables, did not reduce the number of gastric tumors in *nrf2*-disrupted mice, but had a protective effect in wild-type mice when administered in the diet before and during B[*a*]P exposure. Collectively, these results highlight the prime importance of elevated phase 2 gene expression in the cancer chemopreventive actions of oltipraz and sulforaphane.

Nonetheless, multiple studies have shown that oltipraz is also an inhibitor of some cytochrome P450 enzymes, such as CYP1A1/2, CYP1B1, CYP3A4 and CYP2E1 (28–31). A time-course analysis in primary cultures of rat hepatocytes showed that inhibition of ethoxyresorufin-*O*-deethylase (EROD) activity (associated with CYP1A1/2) by oltipraz was detectable after 40 min and maximal between 2 and 12 h of exposure (28). Inhibition of the bioactivation of B[*a*]P could be envisioned to contribute to the chemopreventive actions of oltipraz. This possibility was assessed in a tumorigenesis study by administering oltipraz 1 h before dosing with B[*a*]P to *nrf2*-deficient mice. To further characterize the role of *nrf2* genotype on B[*a*]P disposition, we measured the levels of B[*a*]P–DNA adducts in target (forestomach) and non-target tissues (liver) of wild-type and *nrf2*-deficient mice treated with either vehicle or oltipraz 1 or 48 h prior to the carcinogen. Our results on modulation of B[*a*]P–DNA binding and tumor burden of the forestomach of wild-type and *nrf2*-deficient mice give further evidence for the *in vivo* role of the Nrf2 transcription factor in regulating susceptibility to chemical-induced carcinogenesis.

Material and methods

Chemicals

B[*a*]P and other chemicals were purchased from Sigma Chemical Co. (St Louis, MO). B[*a*]P metabolite standards were obtained from the National Cancer Institute Chemical Carcinogen Reference Standard Repository (Midwest Research Institute, Kansas City, MO). 5-(2-Pyrazinyl)-4-methyl-1,2-dithiole-3-thione (oltipraz) was provided by the Division of Cancer Prevention, National Cancer Institute. High-pressure liquid chromatography (HPLC)-grade water, methanol and ethyl acetate were purchased from J.T. Baker (Phillipsburg, NJ). HCl (Ultrapurex) and NaOH (1 N Titrisol) were obtained from EM Science (Gibbstown, NJ). The enzymes for DNA purification, proteinase K and RNase A were obtained from Boehringer Mannheim Biochemical (Indianapolis, IN).

Animals and treatments

Nrf2-disrupted mice were generated as described by Itoh *et al.* (11) and genotypes of homozygous wild-type and *nrf2*-deficient mice were confirmed as reported previously (26). For the DNA adduct studies, female mice (7–9 weeks old), fed AIN-76A diet and water *ad libitum*, were treated with a single dose of oltipraz (500 mg/kg in 0.1 ml of 1% cremophor and 25% glycerol) or vehicle only by gavage, 1 or 48 h before dosing with B[*a*]P (100 mg/kg in 0.2 ml corn oil, p.o.). Mice were killed 24 h after B[*a*]P treatment and DNA was isolated from forestomach and liver tissues as described below. For the carcinogenesis study, female *nrf2*-deficient mice (7–9 weeks old) were randomized into groups of 20 mice and fed AIN-76A diet and water *ad libitum*. Animals were given oltipraz or vehicle by gavage and B[*a*]P was given 1 h later by oral intubation. This sequence of oltipraz and B[*a*]P administration was repeated once a week for a total of 4 weeks. Animals were weighed weekly and killed 30 weeks after the initial treatment. Forestomach tissues were removed and fixed in 10%-buffered formalin solution. Tumors of the forestomach were counted grossly as described by Wattenberg (32). Experiments on animals were conducted in compliance with protocols approved by the Animal Care and Use Committee of the Johns Hopkins Medical Institutions.

DNA isolation from tissues and hydrolysis

Tissues were homogenized in 50 mM Tris–HCl, 10 mM $MgCl_2$, 25 mM KCl, 0.25 M sucrose buffer, pH 7, and centrifuged at 300 *g* for 10 min. Supernatants were discarded and pellets resuspended in Triton X-100-Tris–sucrose buffer and centrifuged at 500 *g* for 10 min, twice. Pellets were resuspended in Tris–sucrose buffer and incubated with 1% sodium dodecyl sulfate and proteinase K (300 μg/ml) for 6 h at 56°C. To improve the recovery of DNA from a single forestomach, the suspension was extracted twice with chloroform:isoamyl alcohol (24:1) and DNA was precipitated from the aqueous phase with ice-cold ethanol. The DNA was then dissolved in Tris buffer, 40 mM NaCl, 5 mM EDTA, pH 7, and incubated with RNase A (100 μg/ml) for 1 h at 37°C. DNA was extracted two more times with chloroform:isoamyl alcohol (24:1), precipitated with ice-cold ethanol after the addition of 1/10 vol of 3 M sodium acetate, pH 5.3, and washed three times with 70% ethanol. DNA was dissolved in H_2O and the concentration was estimated spectrophotometrically by measurement of UV absorbance ratio at 260/280 nm.

B[*a*]P-tetrols were released by acid hydrolysis of DNA (~150 μg) isolated from mouse forestomach and liver at 80°C for 4 h in a final concentration of 0.01 NHCl and stored at −20°C until analyzed by a reverse-phase HPLC-fluorometric method (33). Before injection, an aliquot of the sample was taken for analysis of guanine. The B[*a*]P-tetrols were extracted with saturated ethyl acetate, dried down with a stream of N_2, resuspended in 20% methanol for analysis.

HPLC fluorometric analysis of B[a]P-tetrols and guanine

Analysis of B[*a*]P-tetrols by HPLC was performed with a Hewlett Packard Series 1050 System with an autosampler coupled to an automated gradient controller and a solvent delivery system. All solvents were filtered through 0.22 μm Millipore membranes, degassed under vacuum prior to use and continuously sparged with high purity He throughout the analyses (34). Separations performed with a Luna C18 (Phenomenex, Torrance, CA) reverse phase column (5 μm, 250×4.6 mm) were carried out at 25°C with a flow rate of 0.7 ml/min using a methanol/water linear gradient. Initial solvent conditions were 55% methanol in water with a linear gradient to 75% in 35 min, a linear gradient to 100% methanol in 10 min, followed by 10 min at 100% methanol, then a linear gradient to 55% methanol in 5 min and 20 min at 55% methanol before the next injection. The B[*a*]P-tetrols were detected with a HP 1046A programmable fluorescence detector. The excitation wavelength was set at 246 nm and the emission was measured at 393 nm, after trapping and scanning a B[*a*]P-tetrol standard in the fluorescence flow cell. Quantification was by comparison with a standard curve using authentic B[*a*]P-tetrol standards analyzed prior to and immediately following the analysis of each set of samples. The lower limit of detection with the instrumentation used was 2 pg of *trans-anti*-B[*a*]P-tetrol (TA) and ~3 pg of the other three tetrols. B[*a*]P-triol (*r*-7,*t*-8,*c*-9-trihydroxy-7,8,9,10-dihydrobenzo[*a*]pyrene) was used as an internal standard due to its similar chemical properties to the tetrols. The internal standard was added to each sample before ethyl acetate extraction to detect variations in extraction recovery and fluorometric analysis. Silanized, amber, high recovery autosampler vials were prepared so that 100 μg of hydrolyzed DNA would be injected in a 200 (liver) or 220 μl (forestomach) injection. Levels of B[*a*]P-tetrols released from mouse forestomach and liver were expressed as picomole per micromole guanine.

Guanine from ~1 μg DNA per injection was eluted from a Whatman Partisil 10 SCX column, isocratically, with 50 mM ammonium phosphate buffer pH 2, at a flow rate of 1 ml/min. Guanine was detected with the excitation wavelength set at 246 nm and the emission was measured at 354 nm. Levels of guanine were determined by comparison with a standard curve using authentic guanine standard in 0.01 N HCl (35).

Statistical analysis

Statistical significance was determined by one-way ANOVA followed by Tukey's multiple comparison. Experimental values are given as mean ± SE.

Results

Effect of oltipraz treatment on B[a]P-induced neoplasia of the forestomach

In order to evaluate the possible role of P450 inhibition by oltipraz on B[*a*]P-induced neoplasia of the forestomach, female *nrf2*-deficient mice were treated weekly with oltipraz or vehicle only 1 h before B[*a*]P administration. This sequence of dosing was done for 4 consecutive weeks and animals were killed 30 weeks after the initial treatment. Initial mean body weights of both vehicle- and oltipraz-treated *nrf2*-deficient mice (22.8 ± 1.9 and 22.4 ± 1.6 g, respectively) were similar to those in the 48 h oltipraz pre-treatment experiment (22.1 ± 2.1 and 22.4 ± 2.1 g, respectively). The body weight gains at the end of the 30-week experiment were 8.7 and 7.4 g for *nrf2*-disrupted vehicle- and oltipraz-pre-treated groups (1 h), respectively, compared with 8.6 and 7.9 g in the 48 h pre-treatment experiment (26). Therefore, we observed no difference on

Table I. Effect of oltipraz treatment on B[*a*]P-induced neoplasia of the forestomach of wild-type and *nrf2*-deficient mice

Genotype	Treatment	Interval between oltipraz and B[*a*]P			
		1 h		48 h[d]	
Wild-type	Vehicle	N.D.[a]		9.5 ± 1.0 (n = 14)	$P < 0.01$
	Oltipraz	N.D.		4.6 ± 0.5 (n = 18)	
nrf2-deficient	Vehicle	29.7 ± 1.7[b] (n = 10)[c]	$P = 0.83$	14.1 ± 1.2 (n = 14)	$P = 0.98$
	Oltipraz	29.2 ± 1.7 (n = 12)		13.6 ± 1.1 (n = 16)	

[a]Not done.
[b]Gastric tumor per mouse ± SE.
[c]Number of mice at risk at termination of experiment.
[d]From reference (26).

body weight gains by oltipraz treatment, pre-treatment intervals or by genotype. As observed previously, several animals from each group died before the end of the 30-week experiment with symptoms of respiratory distress. Upon autopsy, the thymus was found to be enlarged, occupying most of the thoracic space and compressing the lungs against the posterior wall. Overall survival rate and tumor morphology were also similar to those obtained in a previous study (26). In the *nrf2*-deficient vehicle-treated group, six mice died between the 17th and 28th weeks, each with between 25 and 35 gastric tumors. An additional mouse had a tumor burden too numerous to count. In the *nrf2*-disrupted oltipraz-treated group, five mice died between weeks 19 and 27, with 27–35 tumors, whereas an additional mouse had a tumor burden too extensive to count. Two animals in the vehicle-treated group and one mouse in the oltipraz-treated group did survive the 30-week experimental period but had such extensive tumor formation that an accurate tumor count was not possible. All animals in both *nrf2*-deficient groups bore tumors. There were no tumor-related early deaths. However, comparing the tumors of those animals that died before the end of the 30-week experiment, it was observed that tumors progressed from individual large pinpoint excrescences to cauliflower growths. As shown in Table I, oltipraz treatment had no protective effect on tumor multiplicity in the forestomach of *nrf2*-deficient mice under these experimental conditions ($P = 0.83$). Both *nrf2*-disrupted vehicle- and oltipraz-treated mice had similar numbers of neoplasms of the forestomach (29.7 ± 1.7 and 29.2 ± 1.7, respectively). For purpose of comparison, the number of gastric tumors per mouse obtained when animals were treated with oltipraz 48 h before dosing with B[*a*]P in an earlier experiment were also included (26). In this initial experiment, *nrf2*-deficient mice had more and larger tumors than wild-type mice. Moreover, oltipraz had no effect on gastric tumor burden in the *nrf2*-deficient mice. The results were the same when tumor yield from animals before the scheduled termination of the experiment were included in the analysis.

Effect of nrf2 genotype and oltipraz treatment on B[a]P–DNA adducts

To examine the effect of *nrf2* genotype and oltipraz treatment on formation of B[*a*]P–DNA adducts, an early step in the process of carcinogenesis, wild-type and *nrf2*-disrupted mice were treated with vehicle or oltipraz 1 or 48 h before the carcinogen and killed 24 h after dosing with B[*a*]P. Time-course studies by Sticha *et al.* (34) indicated that 24 h was the point of highest tetrol burden in the liver of B[*a*]P-treated

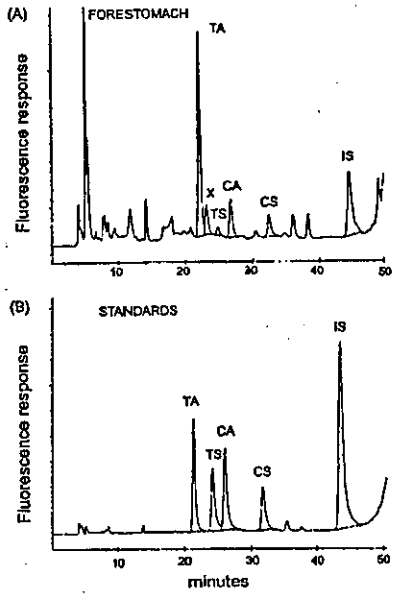

Fig. 1. Representative reverse-phase HPLC-fluorometric profile of the B[*a*]P-tetrols after hydrolysis of DNA isolated from mouse forestomach or liver. (A) Chromatogram of forestomach DNA (100 μg) from a *nrf2*-deficient mouse killed 24 h after B[*a*]P administration. (B) Separation of authentic standards. Details of the animal treatments, and the procedure for isolation and separation of the B[*a*]P-tetrols are given in Material and methods. TA, *trans-anti-*, TS, *trans-syn-*, CA, *cis-anti-*, CS, *cis-syn*-B[*a*]P-tetrol; X, unknown; IS, internal standard.

mice. A representative profile of the tetrol hydrolysis products from forestomach DNA of a *nrf2*-deficient mouse killed 24 h after B[*a*]P administration is shown in Figure 1A. TA was the major tetrol detected in the forestomach and liver of wild-type and *nrf2*-disrupted mice, followed by CS. Peaks other than those corresponding to authentic tetrols standards were also detected, especially a shoulder on the TA. This unknown compound, called X, is likely to be a B[*a*]P metabolite, as it was only found after B[*a*]P treatment and was not detected in DNA from cremophor-glycerol-vehicle and corn oil-vehicle treated animals, nor in DNA from untreated mice. Interestingly, the area under the curve of this peak, relative to the amount of DNA hydrolysate on column, was larger (~4-fold) in chromatograms obtained from the hydrolysis of DNA isolated from forestomach than those obtained from liver samples of the same animal and of the entire treated group. An HPLC

Table II. Effect of *nrf2* genotype and oltipraz treatment on BPDE-DNA adducts

Treatment interval	1 h				48 h			
Genotype	wild-type		*nrf2*-deficient		wild-type		*nrf2*-deficient	
Treatment	vehicle	oltipraz	vehicle	oltipraz	vehicle	oltipraz	vehicle	oltipraz
	B[*a*]P-tetrol (pmol/μmol of guanine)							
Forestomach								
Total tetrols	4.05 ± 0.41[a]	5.50 ± 0.40	10.94 ± 0.50*	14.92 ± 0.82**	4.21 ± 0.25	2.99 ± 0.05*	6.58 ± 0.13*	6.58 ± 0.16
TA	2.18 ± 0.28	2.64 ± 0.21	5.36 ± 0.41*	7.83 ± 0.49**	2.51 ± 0.14	1.81 ± 0.11*	4.33 ± 0.15*	4.34 ± 0.28
CA	0.34 ± 0.03	0.56 ± 0.04	0.98 ± 0.04*	1.26 ± 0.07**	0.41 ± 0.04	0.30 ± 0.02	0.75 ± 0.03*	0.66 ± 0.06
TS	0.73 ± 0.09	0.93 ± 0.05*	1.16 ± 0.08*	1.35 ± 0.09	0.40 ± 0.06	0.26 ± 0.02	0.40 ± 0.03	0.34 ± 0.04
CS	0.80 ± 0.03	1.37 ± 0.15	3.44 ± 0.33*	4.48 ± 0.25**	0.89 ± 0.08	0.62 ± 0.09	1.10 ± 0.12*	1.23 ± 0.24
Liver								
Total tetrols	3.77 ± 0.45	1.32 ± 0.20*	3.12 ± 0.22	2.13 ± 0.16	3.18 ± 0.44	1.65 ± 0.20*	3.29 ± 0.02	2.44 ± 0.20
TA	2.79 ± 0.32	0.92 ± 0.16*	2.33 ± 0.16	1.52 ± 0.16	2.17 ± 0.28	0.98 ± 0.17*	2.50 ± 0.02	1.87 ± 0.10
CA	0.36 ± 0.06	0.16 ± 0.01*	0.30 ± 0.04	0.18 ± 0.02	0.30 ± 0.06	0.18 ± 0.02	0.30 ± 0.04	0.22 ± 0.02
TS	0.21 ± 0.02	0.13 ± 0.00*	0.15 ± 0.01*	0.15 ± 0.00	0.25 ± 0.03	0.17 ± 0.04	0.17 ± 0.02	0.14 ± 0.02
CS	0.41 ± 0.06	0.11 ± 0.00*	0.34 ± 0.02	0.28 ± 0.07	0.46 ± 0.12	0.32 ± 0.05	0.32 ± 0.03	0.21 ± 0.04

[a]Mean ± SE (n = 3 or 4).
*$P < 0.05$, compared with wild-type vehicle-treated mice.
**$P < 0.05$, compared with *nrf2*-deficient vehicle-treated mice.

chromatogram of authentic standards is shown in Figure 1B. B[*a*]P-tetrol standards were also taken through ethyl acetate extraction to determine the efficiency of recovery at different concentrations. The recovery for the four tetrols and B[*a*]P-triol was ~95–99%, over the range of concentrations from 2 to 254 pg.

The results of the analyses in forestomach (target organ) showed that, although not statistically significant, 1 h oltipraz treatment increased the levels of total tetrols in the forestomach of wild-type mice by ~35% (Table II). Similarly, levels of total DNA adducts were significantly increased after oltipraz treatment in the forestomach of *nrf2*-disrupted mice (36%, $P < 0.01$). Analyses of the individual tetrols showed that TA was the major B[*a*]P-tetrol increased by oltipraz, accounting for ~50% of the total increased levels. In both *nrf2*-deficient vehicle- and oltipraz-treated mice levels of total B[*a*]P-tetrols were higher compared with those observed in wild-type mice. In contrast to the results with a 1 h oltipraz pre-treatment, DNA adduct levels were inhibited by 26% ($P = 0.04$) by 48 h oltipraz pre-treatment in the forestomach of wild-type mice. However, this inhibitory effect was not observed in the forestomach of *nrf2*-deficient mice ($P = 1.00$). Both *nrf2*-disrupted vehicle- and oltipraz-treated mice again had higher levels of total DNA adducts than wild-type mice ($P < 0.01$).

In contrast to the results in forestomach tissue, the analyses in liver (non-target organ) of wild-type mice showed that B[*a*]P–DNA adducts were inhibited by 66% ($P < 0.01$) by 1 h oltipraz pre-treatment. Although not statistically significant, this inhibitory effect was also observed in the liver of *nrf2*-deficient mice by 48 h oltipraz pre-treatment (36% inhibition). Interestingly, both *nrf2*-disrupted vehicle- and oltipraz-treated mice had levels of adducts similar to the corresponding wild-type treated mice. No enhancement of hepatic adduct burden was observed in the knockout mice. As in the case of 1 h oltipraz treatment, DNA adduct levels were significantly ($P = 0.01$) inhibited by 49% with 48 h oltipraz pre-treatment in the liver of wild-type mice. Moreover, DNA adducts were also decreased with 48 h oltipraz pre-treatment in the liver of *nrf2* knockout mice (28%, $P = 0.13$).

Discussion

The forestomach was the primary target for B[*a*]P-induced carcinogenesis in the mice (ICR/129Sv background) used in this study and tumor burden could be significantly inhibited when oltipraz was administered to wild-type mice 48 h before the carcinogen (26), in accord with the original findings of Wattenberg and Bueding (1). However, as indicated in Table I, pre-treatment with oltipraz either 1 or 48 h before B[*a*]P was devoid of chemoprotective efficacy in *nrf2*-deficient mice. In addition, these transcription factor knockout mice were intrinsically more sensitive to B[*a*]P carcinogenesis. Therefore, to further characterize the susceptibility of *nrf2*-deficient mice to chemical-induced carcinogenesis, we measured by HPLC-fluorescence detection the interactive effects of *nrf2* genotype and oltipraz treatment on B[*a*]P–DNA adduct levels in the forestomach (target organ) and liver (non-target organ) of wild-type and *nrf2*-deficient mice.

B[*a*]P and its penultimate metabolite, (±)-*trans*-B[*a*]P-7,8-diol require metabolic activation by cytochrome P450s to exert many of their adverse biological effects, including binding to DNA, RNA and proteins, toxicity, mutagenicity and carcinogenicity. Several studies in yeast, baculovirus-infected cells, or in bicistronic systems, have shown that recombinant CYP1A1 was the most active enzyme involved in the oxidation of B[*a*]P, followed by CYP1B1 and to a lesser extent by CYP1A2 and CYP3A4, whereas CYP2C9, CYP2C19 and CYP2E1 formed relatively low amounts of B[*a*]P products (36,37). More recently, using cDNA-based recombinant systems expressing different forms of human cytochrome P450s and NADPH-P450 reductase, Shimada *et al.* (38) showed that CYP1A1 and CYP1B1 had similar catalytic activity toward B[*a*]P and (±)-*trans*-B[*a*]P-7,8-diol. Comparing the metabolism of B[*a*]P and (±)-*trans*-B[*a*]P-7,8-diol by recombinant human P450s in the presence of DNA, Kim *et al.* (37) observed that CYP1A1, CYP1A2 and CYP1B1 each formed the tetrol metabolites of (±)-*trans*-B[*a*]P-7,8-diol with similar stereoselectivity by producing the TA tetrol at the greatest rate. TA is derived from the 7*R*,8*S*,9*S*,10*R*-enatiomer of *anti*-

7,8-dihydroxy-9,10-epoxy-7.8,9,10-tetrahydrobenzo[*a*]pyrene which is the most carcinogenic metabolite formed from (±)-*trans*-B[*a*]P-7,8-diol. Our analyses of B[*a*]P–DNA adducts in mouse tissues were in agreement with this metabolite pattern, as TA was the major B[*a*]P-tetrol detected in DNA isolated from both forestomach and liver of wild-type and *nrf2*-deficient vehicle- and oltipraz-treated mice.

The *in vitro* studies on the metabolic activation of B[*a*]P indicate that CYP1A1 should dominate the oxidation of B[*a*]P in tissues where it is constitutively and inducible expressed. Although, CYP1A1 is expressed predominantly in extrahepatic organs, as well as tumor tissues, it is also highly induced in liver by polyeychic aromatic hydrocarbons (39,40). Studies on the expression patterns of cytochrome P450s failed to detect either constitutive expression of CYP1A1 and CYP1A2 mRNAs by *in situ* hybridization or their protein catalytic activities (EROD, methoxyresorufin-*O*-deethylase) in the stomach of female untreated C57Bl/6N mice and the forestomach of vehicle-treated male Swiss albino mice, respectively (41,42). Treatment of mice with 3-methylcholanthrene led to induction of CYP1A1, but not CYP1A2, transcripts in the mucosa of the stomach (41). However, this induction was modest compared with the effect in other tissues of the gastrointestinal tract. Effects on CYP1B1 mRNA expression and protein were not measured. This pattern of tissue expression of cytochrome P450s suggests that enzymes other than CYP1A1 and CYP1A2 are involved in the biotransformation of B[*a*]P in the mouse forestomach.

Analysis of B[*a*]P–DNA adduct burden in mouse forestomach showed that the levels of individual or total tetrols were higher in *nrf2*-deficient mice, whether vehicle or oltipraz treated, compared with the corresponding wild-type mice. The increased levels of B[*a*]P–DNA adducts in the forestomach of the knockouts presumably reflect the lower basal expression of phase 2 enzymes contributing to B[*a*]P detoxication. mRNA levels for GSTA1/2, GSTP1/2 and NQO1 and their enzymatic activities are substantially (50–70%) reduced in forestomach of *nrf2*-deficient mice (26). Moreover, inducibility of these and other gene transcripts by oltipraz, while marked (3–7-fold) in wild-type mice, is lost in the knockout mice. Oltipraz had no protective effect on tetrol levels when administered either 1 or 48 h before B[*a*]P in the knockout mice. Moreover, reduction in tetrol levels in forestomach DNA of wild-type mice was only observed when oltipraz was administered 48 h, but not 1 h, in advance of the carcinogen. Collectively, these results indicate that the protective actions of oltipraz against B[*a*]P carcinogenesis in the forestomach were mediated by altering phase 2 gene expression without any contribution through inhibition of cytochrome P450 enzymes. This expectation is consistent with our observation that pre-treatment of mice with oltipraz 1 h before B[*a*]P had no protective effect against tumorigenesis. The isoforms of CYP inhibited to the greatest extent by oltipraz are not expressed in this target organ.

CYP1A2 is expressed predominantly in liver. Recent studies reported that CYP 1A1 and 1B1 are also constitutively expressed, albeit at very low levels, in the liver of *AhR* knockout and C57Bl/6J mice (43,44). Hence, this tissue expression pattern suggests that CYP1A1, CYP1B1, CYP1A2, as well as CYP3A4, and CYP2C enzymes activate B[*a*]P in the liver of wild-type and *nrf2*-deficient mice and, for some isoforms (CYP1A1, CYP1A2, CYP3A4) could be affected by oltipraz treatment (29). Indeed, in contrast to the findings in forestomach, oltipraz treatment reduced the levels of hepatic

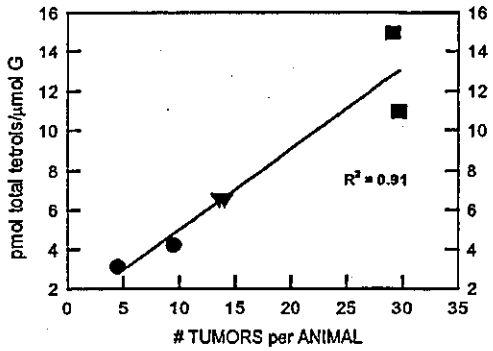

Fig. 2. Correlation between levels of DNA adducts and tumor burden in the mouse forestomach. Circles, wild-type mice; triangle and square symbols, *nrf2*-deficient mice.

B[*a*]P–DNA adducts in (i) animals pre-treated at both 1 and 48 h and (ii) both genotypes of mice. In fact, reductions in tetrol content of hepatic DNA were slightly greater at 1 h pre-treatment with oltipraz than at 48 h, suggesting that inhibition of cytochrome P450s may contribute substantively to the reductions in DNA damage. This mechanism might assume importance under circumstances in which first pass metabolism of B[*a*]P in the liver affects the qualitative and quantitative distribution of B[*a*]P and its metabolites to distal target tissues, such as the lung and bone marrow.

Overall, inhibition of B[*a*]P–DNA adduct burden was 26% ($P = 0.04$) in forestomach when oltipraz was administered 48 h before carcinogen; this level of reduction was also seen for each of the four individual tetrol products. However, inhibition of tumor multiplicity was ~50% ($P < 0.01$) in two studies using identical dosing protocols as the adduct study (1,26). There are other examples where reduction in target organ DNA adduct burden underestimates chemopreventive efficacy of an intervention with oltipraz. Oltipraz is an effective inhibitor of aflatoxin-induced hepatocarcinogenesis; however, dose–response experiments consistently indicate that near complete abrogation of tumor burden is reflected in 60–80% reductions in hepatic levels of aflatoxin–DNA adducts (45). Similarly, Sticha *et al.* (34) have observed that changes in B[*a*]P–DNA adduct levels by the chemopreventive agents benzyl isothiocyanate and phenethyl isothiocyanate do not fully account for their effects on B[*a*]P-induced lung tumorigenesis. The underestimate in the present study may reflect inhibition by oltipraz of other actions of B[*a*]P metabolites, such as cytotoxicity, on the carcinogenic process. Nevertheless, combining all treatments and genotypes, a strong positive linear correlation ($R^2 = 0.91$) was observed between the levels of total B[*a*]P-tetrols and the number of gastric tumors per mouse (Figure 2).

In conclusion, using B[*a*]P as a model chemical carcinogen, our results expand the evidence that the determination of chemical-specific markers for DNA damage, measured here as individual B[*a*]P-tetrols, provide a mechanistic linkage between exposure and disease outcome as well as a monitor for the efficacy of a chemopreventive intervention. Different effects of oltipraz on the levels of B[*a*]P–DNA adducts in target and non-target tissues were observed. Although oltipraz appeared to reduce DNA adducts in a manner consistent with inhibition of cytochrome P450 in liver, such an effect was not observed in forestomach due to lack of expression of susceptible cytochrome P450s. The lack of protective effect of oltipraz

when administered 1 h before B[*a*]P, coupled with the complete abrogation of its protective effects when administered to *nrf2*-disrupted mice 48 h before B[*a*]P, strongly indicates that the anticarcinogenic activity of oltipraz in forestomach can be fully accounted for by modulation of Nrf2-regulated genes. Further understanding of the factors controlling the fate of Nrf2 and its downstream effects, should provide insight and opportunities for the development of effective chemopreventive agents.

Acknowledgements

This work was supported by National Institutes of Health R01 Grants CA 39416, CA 94076 and Center Grant ES 03819. M.R.-G. was partially supported by the Consejo de Ciencia y Tecnologia del Estado de Queretaro (CONCYTEQ) and the Universidad Autonoma de Queretaro, Mexico.

References

1. Wattenberg,L.W. and Bueding,E. (1986) Inhibitory effects of 5-(2-pyrazinyl)-4-methyl-1,2-dithiol-3-thione (Oltipraz) on carcinogenesis induced by benzo[*a*]pyrene, diethylnitrosamine and uracil mustard. *Carcinogenesis*, **7**, 1379–1381.
2. Kensler,T.W. and Helzlsouer,K.J. (1995) Oltipraz: clinical opportunities for cancer chemoprevention. *J. Cell. Biochem. Suppl.*, **22**, 101–107.
3. Benson,A.B., 3rd (1993) Oltipraz: a laboratory and clinical review. *J. Cell. Biochem. Suppl.*, **17**: 278–291.
4. De Long,M.J., Prochaska,H.J. and Talalay,P. (1986) Induction of NAD(P)H:quinone reductase in murine hepatoma cells by phenolic antioxidants, azo dyes and other chemoprotectors: a model system for the study of anticarcinogens. *Proc. Natl Acad. Sci. USA*, **83**, 787–791.
5. Clapper,M.L. (1998) Chemopreventive activity of oltipraz. *Pharmacol. Ther.*, **78**, 17–27.
6. Egner,P.A., Gange,S.J., Dolan,P.M., Groopman,J.D., Munoz,A. and Kensler,T.W. (1995) Levels of aflatoxin-albumin biomarkers in rat plasma are modulated by both long-term and transient interventions with oltipraz. *Carcinogenesis*, **16**, 1769–1773.
7. Rushmore,T.H., Morton,M.R. and Pickett,C.B. (1991) The antioxidant responsive element. Activation by oxidative stress and identification of the DNA consensus sequence required for functional activity. *J. Biol. Chem.*, **266**, 11632–11639.
8. Prestera,T., Zhang,Y., Spencer,S.R., Wilczak,C.A. and Talalay,P. (1993) The electrophile counterattack response: protection against neoplasia and toxicity. *Adv. Enzyme Regul.*, **33**, 281–296.
9. Wasserman,W.W. and Fahl,W.E. (1997) Functional antioxidant responsive elements. *Proc. Natl Acad. Sci. USA*, **94**, 5361–5366.
10. Venugopal,R. and Jaiswal,A.K. (1996) Nrf1 and Nrf2 positively and c-Fos and Fra1 negatively regulate the human antioxidant response element-mediated expression of NAD(P)H:quinone oxidoreductase1 gene. *Proc. Natl Acad. Sci. USA*, **93**, 14960–14965.
11. Itoh,K., Chiba,T., Takahashi,S. *et al.* (1997) An Nrf2/small Maf heterodimer mediates the induction of phase II detoxifying enzyme genes through antioxidant response elements. *Biochem. Biophys. Res. Commun.*, **236**, 313–322.
12. Moi,P., Chan,K., Asunis,I., Cao,A. and Kan,Y.W. (1994) Isolation of NF-E2-related factor 2 (Nrf2), a NF-E2-like basic leucine zipper transcriptional activator that binds to the tandem NF-E2/AP1 repeat of the beta-globin locus control region. *Proc. Natl Acad. Sci. USA*, **91**, 9926–9930.
13. Marini,M.G., Chan,K., Casula,L., Kan,Y.W., Cao,A. and Moi,P. (1997) hMAF, a small human transcription factor that heterodimerizes specifically with Nrf1 and Nrf2. *J. Biol. Chem.*, **272**, 16490–16497.
14. Nguyen,T., Huang,H.C. and Pickett,C.B. (2000) Transcriptional regulation of the antioxidant response element. Activation by Nrf2 and repression by MafK. *J. Biol. Chem.*, **275**, 15466–15473.
15. Chan,K., Lu,R., Chang,J.C. and Kan,Y.W. (1996) NRF2, a member of the NFE2 family of transcription factors, is not essential for murine erythropoiesis, growth and development. *Proc. Natl Acad. Sci. USA*, **93**, 13943–13948.
16. Chan,J.Y. and Kwong,M. (2000) Impaired expression of glutathione synthetic enzyme genes in mice with targeted deletion of the Nrf2 basic-leucine zipper protein. *Biochim. Biophys. Acta*, **1517**, 19–26.
17. Hayes,J.D., Chanas,S.A., Henderson,C.J., McMahon,M., Sun,C., Moffat,G.J., Wolf,C.R. and Yamamoto,M. (2000) The Nrf2 transcription factor contributes both to the basal expression of glutathione *S*-transferases in mouse liver and to their induction by the chemopreventive synthetic antioxidants, butylated hydroxyanisole and ethoxyquin. *Biochem. Soc. Trans.*, **28**, 33–41.
18. McMahon,M., Itoh,K., Yamamoto,M., Chanas,S.A., Henderson,C.J., McLellan,L.I., Wolf,C.R., Cavin,C. and Hayes,J.D. (2001) The Cap'n'Collar basic leucine zipper transcription factor Nrf2 (NF-E2 p45-related factor 2) controls both constitutive and inducible expression of intestinal detoxification and glutathione biosynthetic enzymes. *Cancer Res.*, **61**, 3299–3307.
19. Chanas,S.A., Jiang,Q., McMahon,M. *et al.* (2002) Loss of the Nrf2 transcription factor causes a marked reduction in constitutive and inducible expression of the glutathione *S*-transferase *Gsta1*, *Gsta2*, *Gstm1*, *Gstm2*, *Gstm3* and *Gstm4* genes in the livers of male and female mice. *Biochem. J.*, **365**, 405–416.
20. Chan,K. and Kan,Y.W. (1999) Nrf2 is essential for protection against acute pulmonary injury in mice. *Proc. Natl Acad. Sci. USA*, **96**, 12731–12736.
21. Cho,H.Y., Jedlicka,A.E., Reddy,S.P., Kensler,T.W., Yamamoto,M., Zhang,L.Y. and Kleeberger,S.R. (2002) Role of NRF2 in protection against hyperoxic lung injury in mice. *Am. J. Respir. Cell Mol. Biol.*, **26**, 175–182.
22. Aoki,Y., Sato,H., Nishimura,N., Takahashi,S., Itoh,K. and Yamamoto,M. (2001) Accelerated DNA adduct formation in the lung of the Nrf2 knockout mouse exposed to diesel exhaust. *Toxicol. Appl. Pharmacol.*, **173**, 154–160.
23. Chan,K., Han,X.D. and Kan,Y.W. (2001) An important function of Nrf2 in combating oxidative stress: detoxification of acetaminophen. *Proc. Natl Acad. Sci. USA*, **98**, 4611–4616.
24. Enomoto,A., Itoh,K., Nagayoshi,E., Haruta,J., Kimura,T., O'Connor,T., Harada,T. and Yamamoto,M. (2001) High sensitivity of Nrf2 knockout mice to acetaminophen hepatotoxicity associated with decreased expression of ARE-regulated drug metabolizing enzymes and antioxidant genes. *Toxicol. Sci.*, **59**, 169–177.
25. Braun,S., Hanselmann,C., Gassmann,M.G., auf dem Keller,U., Born-Berclaz,C., Chan,K., Kan,Y.W. and Werner,S. (2002) Nrf2 transcription factor, a novel target of keratinocyte growth factor action which regulates gene expression and inflammation in the healing skin wound. *Mol. Cell. Biol.*, **22**, 5492–5505.
26. Ramos-Gomez,M., Kwak,M.K., Dolan,P.M., Itoh,K., Yamamoto,M., Talalay,P. and Kensler,T.W. (2001) Sensitivity to carcinogenesis is increased and chemoprotective efficacy of enzyme inducers is lost in *nrf2* transcription factor-deficient mice. *Proc. Natl Acad. Sci. USA*, **98**, 3410–3415.
27. Fahey,J.W., Haristoy,X., Dolan,P.M., Kensler,T.W., Scholtus,I., Stephenson,K.K., Talalay,P. and Lozniewski,A. (2002) Sulforaphane inhibits extracellular, intracellular and antibiotic-resistant strains of *Helicobacter pylori* and prevents benzo[*a*]pyrene-induced stomach tumors. *Proc. Natl Acad. Sci. USA*, **99**, 7610–7615.
28. Langouet,S., Maheo,K., Berthou,F., Morel,F., Lagadic-Gossman,D., Glaise,D., Coles,B., Ketterer,B. and Guillouzo,A. (1997) Effects of administration of the chemoprotective agent oltipraz on CYP1A and CYP2B in rat liver and rat hepatocytes in culture. *Carcinogenesis*, **18**, 1343–1349.
29. Langouet,S., Furge,L.L., Kerriguy,N., Nakamura,K., Guillouzo,A. and Guengerich,F.P. (2000) Inhibition of human cytochrome P450 enzymes by 1,2-dithiole-3-thione, oltipraz and its derivatives and sulforaphane. *Chem. Res. Toxicol.*, **13**, 245–252.
30. Sofowora,G.G., Choo,E.F., Mayo,G., Shyr,Y. and Wilkinson,G.R. (2001) *In vivo* inhibition of human CYP1A2 activity by oltipraz. *Cancer Chemother. Pharmacol.*, **47**, 505–510.
31. Le Ferrec,E., Ilyin,G., Maheo,K., Bardiau,C., Courtois,A., Guillouzo,A. and Morel,F. (2001) Differential effects of oltipraz on CYP1A and CYP2B in rat lung. *Carcinogenesis*, **22**, 49–55.
32. Wattenberg,L.W. (1977) Inhibition of carcinogenic effects of polycyclic hydrocarbons by benzyl isothiocyanate and related compounds. *J. Natl Cancer Inst.*, **58**, 395–398.
33. Alexandrov,K., Rojas,M., Geneste,O., Castegnaro,M., Camus,A.M., Petruzzelli,S., Giuntini,C. and Bartsch,H. (1992) An improved fluorometric assay for dosimetry of benzo(*a*)pyrene diol-epoxide-DNA adducts in smokers' lung: comparisons with total bulky adducts and aryl hydrocarbon hydroxylase activity. *Cancer Res.*, **52**, 6248–6253.
34. Sticha,K.R., Staretz,M.E., Wang,M., Liang,H., Kenney,P.M. and Hecht,S.S. (2000) Effects of benzyl isothiocyanate and phenethyl isothiocyanate on benzo[*a*]pyrene metabolism and DNA adduct formation in the A/J mouse. *Carcinogenesis*, **21**, 1711–1719.
35. Herron,D.C. and Shank,R.C. (1982) DNA methylation during chronic administration of 1,2-dimethylhydrazine in a carcinogenic regimen. *Carcinogenesis*, **3**, 857–860.
36. Bauer,E., Guo,Z., Ueng,Y.F., Bell,L.C., Zeldin,D. and Guengerich,F.P. (1995) Oxidation of benzo[*a*]pyrene by recombinant human cytochrome P450 enzymes. *Chem. Res. Toxicol.*, **8**, 136–142.